Feasibility of Measuring Nuclear Moments and Radii with Laser Spectroscopy and the RPMS

P. Dyer

The MSU superconducting cyclotron, providing intense beams of heavy ions, and the reaction product mass separator (RPMS) for energetic reaction products will provide a forefront facility for the study of short-lived nuclei far from the line of beta stability. We are initiating a program to measure some of the most fundamental properties of the ground states (or isomers) of such nuclei: the radii, spins, magnetic moments, and quadrupole moments, through the study of the hyperfine structure of optical transitions of the atoms.

The hyperfine structure of atomic states arises from the interaction of nuclear magnetic and quadrupole moments with the atomic electrons. Nuclear moments may be determined from the spacings of the atomic levels; nuclear spins may sometimes be determined from the number of these levels. In addition, changes in the root-mean-square radius between two isotopes may be determined by measuring the difference in the location of the centroids of the multiplets; these isotope shifts provide an alternative method for measuring nuclear deformations. The location of regions of deformation and regions of closed-shell nuclei for nuclei far from stability will be one of the major interests in performing laser-spectroscopy experiments at MSU, as nuclei with a broad range of atomic numbers and masses may be studied.

Proton-rich nuclei may be produced by heavy-ion-induced fusion reactions; neutron-rich nuclei may be produced by deeply inelastic ($\lesssim$20 MeV/nucleon) or fragmentation ($\gtrsim$20 MeV/nucleon) reactions. During operation of the first superconducting cyclotron (Phase I), it is expected that fusion reactions will produce the highest yields of nuclei far from stability at the focal plane of the RPMS (yields of the order of 10^5/sec), whereas with the addition of a second cyclotron (Phase II) in the mid-1980's, the highest focal plane yields will be produced by fragmentation reactions; these fragmentation yields are expected to be significantly higher than those of the Phase I fusion reactions: up to 10^8/sec.

For laser spectroscopy the reaction products will have to be slowed down and neutralized at the focal plane of the RPMS. The products will then intersect the beam from a dye laser pumped by an ion laser. Excitation of the atomic states can then be detected in one of several ways. Two of the techniques we plan to use are (1) detection of the fluorescence radiation and (2) detection of an anisotropy in the angular distribution of nuclear decay products which is produced by optical pumping with circularly polarized laser light.

The most sophisticated dye laser available commercially today is an actively stabilized CW ring dye laser which can be run single mode, and which can be automatically scanned in frequency. Such a laser is pumped by an argon or krypton ion laser having a total output power of up to 20 watts. The laser medium is a jet of liquid in which is dissolved one of several dyes, depending on the desired wavelength. Large dye molecules have many narrowly-spaced vibrational and rotational levels which are broadened in the solvent environment, so that the fluorescence forms a broad continuum over a spectral range of typically 50 to 100 Å. Such a laser system can be continuously tuned from 4100 Å to 8000 Å, with single-frequency powers sometimes greater than 1 watt. The linewidth is less than 1 MHz (about 1.5×10^{-5} Å). The combination of such high powers for a monochromatic source of photons and the large interaction cross sections (up to 10^{14}barns) make possible the detection of single atoms with some techniques.

Fairbank et al.[1] have compiled a table of ground-state transitions for 87 elements for which the atomic energy levels are known, the entries being those transitions most promising for use in the resonance fluorescence method. Forty elements are in the range of 4200 to 7800 Å, which is readily accessible with present dye lasers. Twenty-three more may be readily reached with frequency doubling techniques, 2650 to 4200 Å (see discussion below); 10 more might be reached by frequency doubling, though with greater difficulty, 1780 to 2650 Å; and 14 are not accessible with present techniques, 800 to 2300 Å. (Even some of these elements might still be studied if ions or metastable atoms could be produced in large enough quantitites.) Most of these transitions involve a change in the number of s electrons, so that isotopic shifts may be measured, as well as spins and moments.

Developments in the past year point to the possibility of obtaining tunable, single-frequency, CW ultraviolet laser radiation of power in the milliwatt region. This has been achieved for wavelengths in the 2930 to 3050 Å range by second harmonic generation (frequency doubling) in a ring dye laser.[2] A modified Coherent CR-699-21 dye laser was used, with an ADA crystal positioned at the auxiliary beam

waist and with temperature-tuned phase matching. The maximum powers achieved were 48 mW total and 22 mW locked single frequency.

It is thus seen that with commercial dye lasers, with some extrapolation of frequency doubling development, 63 out of the above 87 elements are accessible to study.

In selecting elements for which it will be easy to do the initial experiments, we apply the conditions that an easily-handled dye be used, that high output power be available, that the transition probability be large, and that the mass number be greater than about 80, so that Doppler broadening is not a serious problem. We eliminate alkalis, as they have been studied extensively elsewhere. With these conditions, the following elements stand out as possibilities for first experiments.

Zr	Z=40
Nd	Z=60
Eu	Z=63
Gd	Z=64
Os	Z=76
U	Z=92

In the first studies, isotopes on the proton rich side would be produced by fusion reactions. Of the above elements, Zr and Gd are interesting cases to study because of possible shell effects; in both cases subshells are closed for the protons. The isotopes ^{90}Zr and ^{146}Gd have neutron closed shells as well.

In designing an experimental configuration for the laser spectroscopy measurements, it is required that there be sufficient overlap between the laser beam and the atoms to be excited. Doppler broadening must be reduced if high-resolution data is to be acquired. In the first experiments we anticipate sending the reaction products through a foil, where most of the kinetic energy will be lost, and then into a cell containing a rare gas such as helium. Since an energy range of about 10% is accepted by the RPMS, even if the least energetic recoils are stopped in the foil, the remaining recoils may still be spread out over a length of several cm when stopped in the gas downstream from the foil. This problem may be overcome by bringing the laser beam in nearly collinearly with the direction of the products. Elliptical mirrors and phototubes can be used to collect the fluorescence radiation. If the stopping gas can be cooled, Doppler broadening can be reduced to some degree. Such a system is adequate for studies of relatively heavy nuclei.

For an alternative, more sophisticated system, the reaction products emerging from the foil can be stopped and excited in a flow of cooled helium (possibly a configuration similar to that of a very short cryogenic helium jet). The Doppler broadening would be reduced; the laser beam could be brought in at 90° to the flow, and most recoils would be swept through the laser beam sooner or later.

For either of these configurations, reduction of background in the phototubes from dark current and scattered light is required if the number of reaction products per second is less than 10^3. This may be achieved by tagging the time of arrival of the reaction product at the focal plane with a transmitting detector. If timing between this detector and the phototube output of 1 msec or better can be obtained, background can be reduced.

Later experiments might include studies of Sn (requiring frequency doubling techniques) and lighter elements such as Mg and Ca. Studies of fission isomers and high-spin isomers should also be possible. It is expected that laser techniques more sophisticated than those described above (such as saturation spectroscopy or laser-rf double-resonance spectroscopy) will be required in many cases.

In order to become acquainted with laser spectroscopic techniques, we are presently collaborating with the group of Dan Murnick at Bell Labs and Rutgers University. We are presently setting up a new laser system at the Rutgers Nuclear Physics Laboratory, where the first measurement is to be the determination of the magnetic moment of the 1^+ state of ^{22}Na at 583 keV ($\tau_{\frac{1}{2}}$ = 352 nsec). The measurement will be similar to that used for the earlier ^{24m}Na experiment at Bell Labs.[3]

The recoiling ^{22m}Na nuclei will pass through a foil, where most of their kinetic energy is to be lost. The recoils will then be thermalized and neutralized in a cell containing about 50 torr of argon gas. The atoms will be polarized via optical pumping with a circularly polarized beam from a dye laser tuned to the resonant frequency of 5890 Å. For right circularly polarized light, the selection rule for absorption is $\Delta M_F = +1$, whereas for spontaneous emission it is $\Delta M_F = 0, \pm 1$. Several excitations will lead to all the atoms being in the maximum M_F level, and because of the coupling by the hyperfine interaction, the nuclei will also be polarized. These polarized nuclei will emit anisotropic gamma radiation. The anisotropy is to be measured with two Ge(Li) detectors as a function of the laser frequency. The position of the atomic resonance will give the magnetic moment, including the sign.

Thus far a beam line and chamber have been constructed, and a table for the laser system has been erected. The required optical elements have been ordered.

---

1. W.M. Fairbank, Jr., T.W. Hansch, A.L. Schawlow, J. Opt. Soc. Am. 65, 199 (1975).
2. Coherent engineering report, Oct. 31, 1979.
3. D.E. Murnick, H.M. Gibbs, O.R. Wood II, L. Zamick, P. Pappas, M. Burns, T. Kuhl, M.S. Feld, Phys. Lett. 88B, 242 (1979).

Attenution of Light in Liquid Organic Scintillators

John E. Yurkon and Aaron Galonsky

The light attenuation characteristics of NE213 and NE224 have been measured over the region of wave lengths from 5200A^{o} through 4100A^{o}. These measurements were performed by using an argon laser to accurately measure the light attenuation at several wave lengths.[1] The light attenuation lengths were also measured in 10A^{o} steps from 5200A^{o} through 4100A^{o} by passing white light through liquid scintillation cells of different lengths and measuring the transmitted light spectra with a SPEX monochrometer. The attenuation lengths measured by the laser method were used to calibrate the data from the SPEX monochrometer.

The light emission spectra of NE213 and NE224 were also measured by exciting the liquid scintillators with short ultraviolet light from the argon laser and measuring the light emission spectra with the SPEC momochrometer. This has been shown by Birks et al.[2] to be equivalent to using an ionizing source of radiation to excite the scintillator.

The wave length dependent light attenuation lengths have been applied to the light emission spectra for NE213 and NE224 to show the total light transmitted versus path length. This data is to be compared with light transmission observed in an actual scintillation counter using a ^{228}Th source when all data analysis is finished.

---

1. J.E. Yurkon and Aaron Galonsky, April 1979, MSUCL-295.
2. J.B. Birks, J.E. Geake, and M.D. Lumb, 1963, J. Chem. Phys., 14, 141.

Comparison of Runge-Kutta and Predictor-Corrector Integration Methods

M. DiStasio and Wm. C. McHarris

Numerical integration techniques have become standard tools in solving differential equations. The number of different techniques available for integration purposes is very great and there are characteristic differences even among algorithms of the same general class. For our purposes we can consider the majority of integration techniques, to divide naturally into two general categories - one-step and multi-step methods. We concern ourselves here with two popular methods that exemplify the basic character and philosophy of the two aforementioned general categories; Runge-Kutta methods as examples of the one-step techniques and predictor-corrector algorithms as members of the multi-step family. These two methods are well-known and documented in a variety of numerical alalysis texts. Yet the practical differences that are of real interest to an experimentalist who is faced with the task of solving an analytically intractable set of differential equations, are not well explained in standard texts. In an effort to demonstrate more clearly the practical differences we have compared a number of different aspects of fifth order Runge-Kutta and the Hamming method of predictor-corrector integration.

To compare the relative speed of the two methods we performed 5000 integration steps for equations of the form $d^2f(x)/dx^2 = g(x,x')$. The results are shown for a number of different f(x) in Table I. Obviously, in these cases, the Runge-Kutta method requires, on the average, 40% more time than the predictor-corrector method.

Table I.

Function	Time of Calculation for 5000 steps (in seconds)		Ratio RK/PC
	Predictor-Corrector	Runge-Kutta	
tanh(x)-x	15	23	1.5
exp(x)-x-1	15	21	1.4
sech(x)-1	16	22	1.4
cosech(x)+	19	31	1.6
cosh(x)-1	15	21	1.4
sinh(x)-x	15	21	1.4
log(x)-x+1	16	22	1.4
x+1/x	16	22	1.4
cos(x)	15	21	1.4
sin(x)	15	20	1.3

Development of a Simulation Program for Heavy Ion Collision Products

B.E. Hasselquist, G.F. Bertsch and G.M. Crawley

One measurement proposed for the analysis of heavy ion collisions from 20-200 MeV/A is that of the coefficients of a spherical harmonic expansion of the angular distribution of the products.[1] In an attempt to assess the feasibility of this measurement in terms of various experimental detector arrangements, a computer simulation program was developed. If we define an angular distribution in the c.m. frame by a fit to the spherical harmonic expansion

$$f(\theta,\phi) \sim Y_o + \sum_{m}^{L>0} \alpha_{Lm} Y_m^L(\theta,\phi) \qquad (1)$$

and fit the distributon function

$$F_{exp}(p) = \sum_{i}^{N} \delta(p-\Omega_i) \qquad (2)$$

for N particles to Eq (1), we find the coefficients to be given by

$$\alpha_{2m}^{exp} = \frac{\sqrt{4\pi}}{N} \sum_{i}^{N} Y_{2m}(\Omega_i). \qquad (3)$$

α^{exp} is calculated twice in the simulation program for each value of m--first using the actual computer generated angles taking the sum over all particles and second using the angles corresponding to the center of the detector array. The second calculation may be done assuming that the detectors may each fire only once for a given event or assuming that all particles are counted individually, the latter case providing a check on the program.

The program generates angles and momentum values for each particle in the c.m. frame. Momentum values are based on a Boltzmann distribution and the angles are derived from an asymmetric generating function of the form

$$f(\theta,\phi) = N(e^{\beta\cos\theta} + e^{-\beta\cos\theta}) \qquad (4)$$

where $\cos\theta = \cos\theta\cos\frac{\pi}{4} + \sin\theta\sin\frac{\pi}{4}\sin\phi$ and where the angle and momentum values are assigned randomly. These values are then transformed into the lab frame where they are sorted according to the particular detector array which has been set up in the program.

Calculations have been done for E_{lab} = 100 MeV/A ^{40}Ar + ^{40}Ar using various detector arrays and for a range of impact parameters. In Fig. 1 we show a comparison of the detected α_{21} with the actual α_{21} for 400 events assuming that all of the twenty particles were detected. Although the histograms are similar and give similar averages there is some variation coming from the experimental angular resolution. If the more realistic assumption is made, that multiple counts in a single detector cannot be distinguished and therefore cannot be used, then we find that the histograms differ significantly (Fig. 2). Thus, this program can be used to investigate various detector arrangements for particular target-projectile systems and bombarding energies.

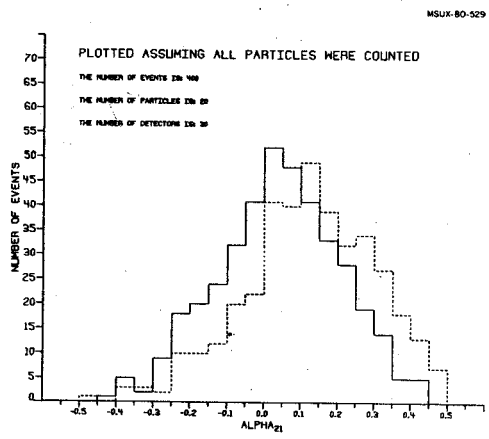

FIG. 1. Comparison of the actual α_{21} (solid histogram) to the detected α_{21} (dashed histogram) assuming all particles are detected. The value of β is 4.96 indicating a strongly asymmetric angular distribution in the c.m. frame.

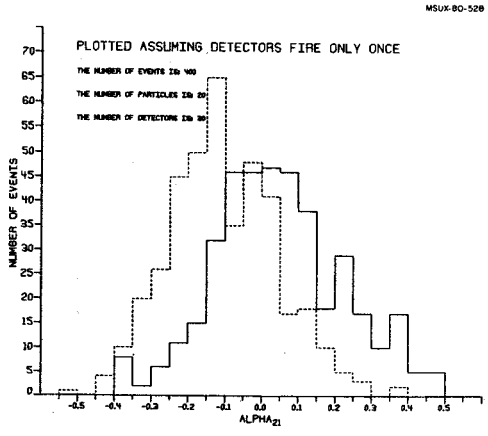

FIG. 2. Same as Fig. 1, assuming the detectors fire only once.

1. G. Bertsch and A.A. Amsden, Phys. Rev. C 18, 1293 (1978).

Comptonless Gamma Ray Spectrometer

J. Kasagi and R.M. Ronningen

It is highly desirable to detect gamma rays without Compton backgrounds, especially for the measurement of the correlations between transition energies of more than one γ-ray.[1] We have tested a NaI-NaI γ-ray sum spectrometer to reduce the Compton background by extending the method of kinematic selection[2,3] of Compton events.

The spectrometer consists of two 2 in. x 2 in. NaI(Tl) detectors. One of them is used as a scatterer, the other, an analyzer. The analyzer detector is placed with the axis perpendicular to the axis of the scatterer. The distance between the γ-ray source and the front end of the scatterer was about 15 cm. A lead block of 12 cm thickness was used to prevent γ-rays from entering the analyzer.

The experiment was performed by using $^{22,24}Na$, ^{60}Co, ^{137}Cs and $^{152+154}Eu$ sources. A conventional fast-slow timing method with a time-to-amplitude (TAC) converter was used to detect coincidences between pulses in the scatterer and in the analyzer. The outputs of the TAC and two amplifiers were fed to three ADC's, and raw data were acquired on mangetic tapes. The off-line analysis was made as follows. First, we calculated the kinematic quantity, F, for each event as follows:

$$F = \frac{m_o c^2 E_s}{E_a(E_a+E_s)}$$

where E_s and E_a are the energies abosrbed in the scatterer and the analyzer, respectively, and $m_o c^2$ is the rest mass of the electron. The quantity F can be used to select the process of the event as discussed in ref. 3. Then we determined the F-gate for the events which mainly contribute the full energy peak (A-gate) in sum spectrum. Finally, we searched for another F-gate (S-gate) which reproduces the Compton background of the spectrum.

Figure 1 shows the F spectrum for the ^{60}Co source. As can be seen, the events corresponding to the backgrounds are distributed throughout a rather broad region in the F spectrum. On the other hand, the F spectrum gated by 1.33 MeV photopeak shows broad peak centered about F = 0.8. The S-gate is determined for several energies to eliminate the background of the spectrum generated by A-gate, using ^{137}Cs, ^{60}Co, ^{24}Na, sources. This empirically determined gate versus γ-ray energy is shown in Fig. 2. In Fig. 3 the sum spectrum gated by the A-gate, and the corrected spectrum for ^{60}Co source. A spectrum for a complex γ-ray decay (^{152}Eu + ^{154}Eu) is shown in Fig. 4. As can be seen from these figures, the Compton event backgrounds can be completely eliminated.

The performance of the spectrometer is summarized in Table 1. The detection efficiency of the spectrometer is not large but it could be increased (numbers in brackets) to about 20% by adding more analyzers. In the last column the number of counts in a 100 keV region below the photopeak is compared to the photo-

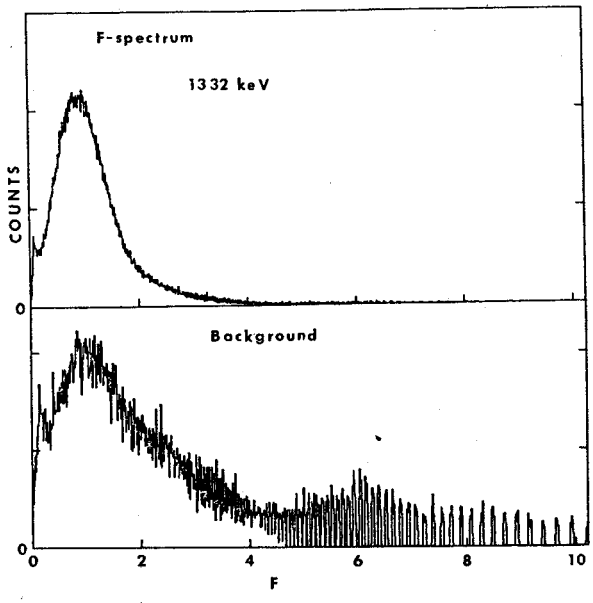

FIG. 1. F spectra contributing only to the photopeak of the 1332-keV γ ray (upper) and contributing to the background region of the summed energy spectrum (lower).

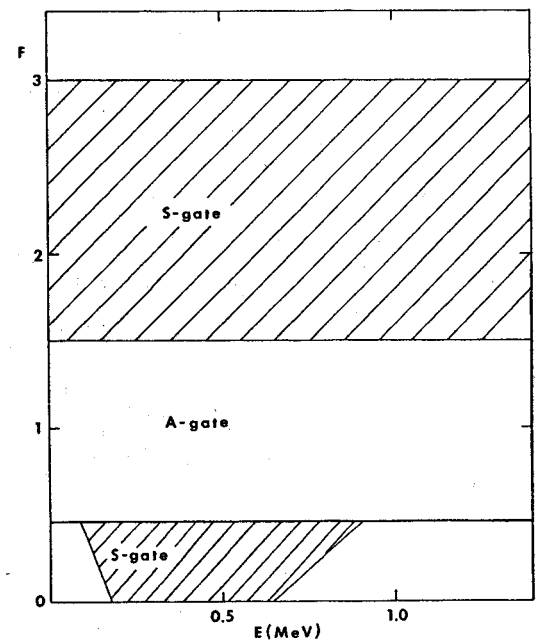

FIG. 2. Plot of the S-gate against E_γ used to subtract the background.

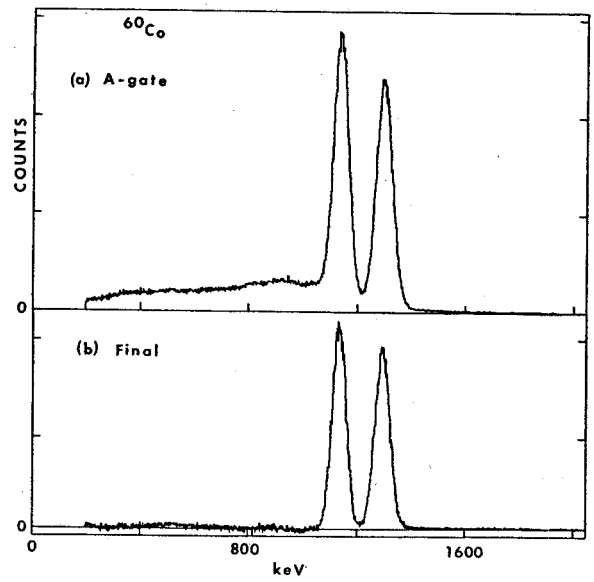

FIG. 3. Energy spectra of ^{60}Co; (a) the summed energy spectrum gated by A-gate and (b) the background subtracted spectrum.

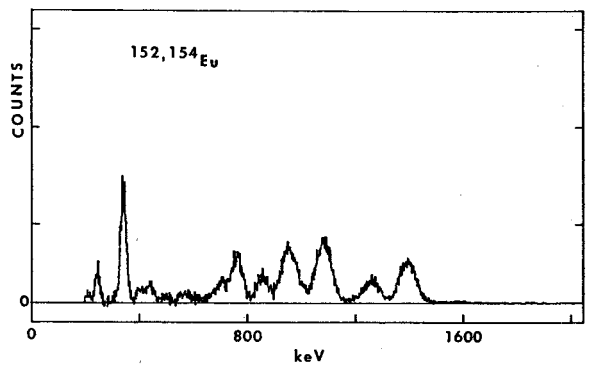

FIG. 4. Energy spectrum of $^{152+154}$Eu.

Table I. Characteristics of a two 2in. x 2 in. NaI(Tl) crystal gamma ray spectrometer. The relative efficiencies in brackets result from assuming more analyzer detectors of the same size are usual. In the last column the number of counts in a 100 keV region below the photopeak is compared to the number of counts in the photopeak. The percentage photopeak fractions are these numbers subtracted from 100%.

E (keV)	Relative Efficiency (%)	Resolution (keV)	$\frac{\Delta N/100\ keV}{N}$ photopeak (%)
662	3 (12)	≃ 45	< 1.3
1332	4.5 (18)	≃ 70	< 1.1
2755	4.5 (18)	≃ 120	< 6.0

peak area. Note that a 99% photopeak efficiency is achieved.

For γ-rays having energies larger than 2 MeV, it was found to be difficult to eliminate the background completely. Figure 5 shows the sum spectrum for the ^{24}Na source. A small bump and dip are evident, whose energies correspond to the energies just below single escape and double escape energies. These are caused by the 511 keV γ-rays that escape the analyzer. Therefore, the difficulty might be resolved by using a larger NaI(Tl) detector as an analyzer.

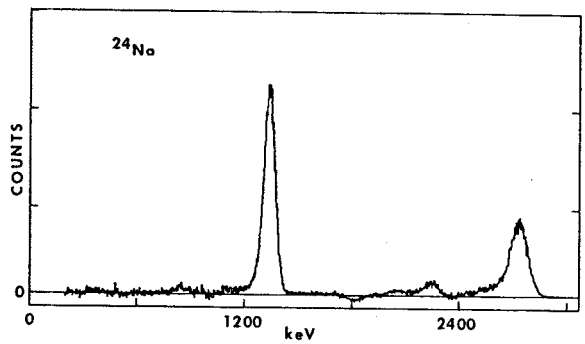

FIG. 5. Energy spectrum of ^{24}Na.

1. O. Anderson et al., Phys. Rev. Lett. 43, 687 (1979).
2. P.A. Butler et al., Nucl. Instr. and Meth. 108 497 (1973).
3. J. Kasagi, N. Kishida and H. Ohnuma, Nucl. Instr. and Meth. 144, 201 (1977).

Progress in the Development of a Detector Laboratory

J.E. Yurkon, G. Poggi, P. Dyer, C.K. Gelbke and T.C. Awes

A facility for the design and testing of gas counters is being developed. To date this includes: a wire winder for the fabrication of wire planes for multi-wire Parallel Plate Avalanche counter; and a foil-stretcher for the production of thin, polypropylene films in the range of 20-100 g/cm^2. This facility has produced a position sensitive Parallel Plate Avanlanche counter, and a single wire proportional counter for the k = 320 low resolution spectrograph.

I. The wire winder

A survey of wire winders in use in North America was made, and it was decided that a design similar to the one in use at Fermi Lab would be the most appropriate for this facility. The design criteria was to have a device capable of placing evenly spaced wires on a plane, up to a meter on a side, with an accuracy of at least 100 microns, and capable of handling fine wire with the tension of the wire adjustable between 5-200 grams.

The wire winder (Photograph 1) consists of a table, containing the tensioning device and wire feed, which rides on ball busing shafts and is driven along the shafts by a precision lead screw. The leadscrew and table assembly in turn ride upon another set of ball bushing shafts so that they may be easily set in proximity to a rotating frame, which can be configured to various dimensions necessitating the moving of the table and lead screw. The rotating frame is driven by a D.C. gearmotor while the lead screw is driven by a stepper motor. The stepper motor moves the table a set distance at each revolution of the frame.

A Z-80 microprocessor handles the acceleration/deceleration and number of steps of the lead screw. It also monitors the wire tensioning device for failures, and checks to see if the table has moved past preset limits. The microprocessor is the only interface the user need be concerned with. The non-volatile program allows the user to set the wire spacing, expressed in millimeters, choose the direction the frame is to be wound, and can run the winder in reverse to save wire if a mistake has been made.

The wire tension consists of a tension arm whose tension is set either by a spring for the range 5-20 grams, and by a motor used as a torque device for the range of 20-200 grams. The wire is fed off a spool by a D.C. control motor which is controlled by a servo-loop consisting of a position sensing element on the tension arm and the motor. A functional block diagram is shown in Fig. 1. This arrangement is necessary to reduce the effects of the inertia of the wire spool. The variance in tension has not yet been measured, but is expected to vary less than 10% worst case.

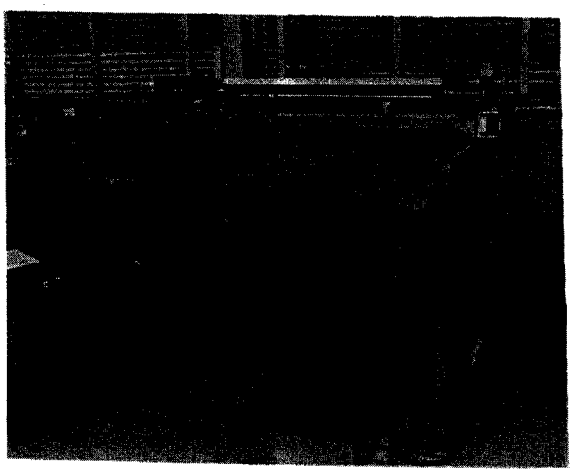

Photo 1. The wire winder and control ray.

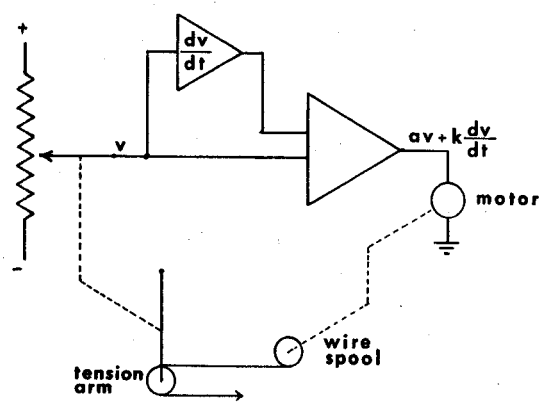

FIG. 1. Block diagram of tension arm servo-loop.

Two test frames have been wound, one with a 1 mm spacing with a tension of 7 grams, the other with a 250 micron spacing. The wire used was 80 micron copper with enamled insulation. Neither frame has been tested for accuracy but a visual inspection of the 250 micron spaced frame suggests an accuracy of better than 100 microns. Twenty microns should be achievable considering stepping motor resolution and lead screw precision.

II. The foil strecher

A foil strecher similar to one constructed at Los Alamos was built.[1] (Photograph 2). An aluminum[2] disk, 45 cm in diameter covered with teflon and heated is raised through a 1 mil polypropylene film to stretch it to thicknesses of 20-100 gm/cm^2. The temperature of the disk is controlled by a center heating element supplied by a variac and the temperature gradient is controlled by grooves cut in the disk. The drive to raise the disk is the only major difference with the Los Alamos design. A pair of pneumatic cylinders raise the disk with the rate controlled by a center hydraulic cylinder. This prevents jerking in the upward travel of the cylinders due to frictional loading.

The motion and temperature control of the stretcher has been tested but no films have been stretched to date due to difficulties in covering the disk with teflon.

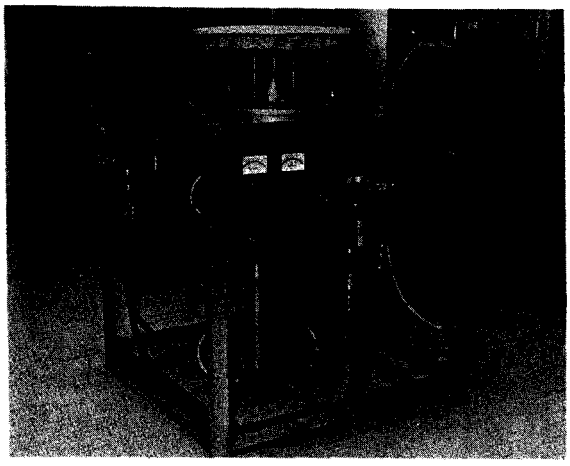

Photo 2. The foil-stretcher.

III. Construction of a position sensitive parallel plate avalanche counter

Good time resolution at high counting rates with a minimum thickness rendered the parallel plate avalanche counter (PPAC) on almost ideal time-sensitive transmission detector for heavy ions.[2,3] In the last few years techniques have been developed in order to obtain from a PPAC also position information;[4,5] one of these techniques consists on inserting in the gap between anode and cathode a sense wire frame biased at half the main electrodes potential difference. Delay line readout is used for extracting position information from the signal sensed by the wires that are close to the location of the avalanche.

Following the outlined scheme we are building a X and Y position sensitive PPAC consisting of two independent elements, one for each direction, the function characteristics are the following:

sensitive area: 16 cm x 20 cm
gap between electrodes: 3 mm
distance between adjacent wires: 1.5 mm
tapped delay line readout
delay per tap: 2 us
pressure range: 4-10 torr
filling gas: isostructure propane
operating voltage: 500-600 volt
expected position resolution: 1 mm

A prototype has been checked at 5 torr propane, 500 biasing voltage for detecting 5.5 MeV particles. Two of these counters will be used for coincident fission fragment detection in connection with the study of light particles emission in central and periphial heavy ion collision in the projectile energy range of few tens of MeV/A.[6]

IV. Single wire proportional counter for l = 320

A single wire proportional counter for the K=320 low resolution spectrometer has been constructed and partially tested. The counter is a transmission counter having two interprior ground plane windows 1.7 cm apart, and .8 mg/cm^2 thick. The two pressure windows are 1.8 mg/cm^2 thick. A .5 mil stainless steel wire is located at the center of the counter. The active area of the detector is .5 cm x 30 cm. The detector is expected to have a .3 mm position resolution when operated at 90 torr of isobutane for 250 MeV α particles.

The linearity of the detector has been tested with 8 MeV α's at normal incidence and shows a differential linearity of better than .6%. When operated at 45 torr of isobutane at 1100 volts the position resolution was 1.8 mm which is the limit of the first collimator used additional testing is required.

---

1. P.N. Bappus, and R.L. Blacke, LA-UR-76-1563; Los Alamos.
2. G. Gaukler, H. Schmidt-Boeking, R. Schuch, R. Schube, H.J. Specht and I. Tserruya, Nucl. Instr. and Meth. 141 (1977) 115.
3. A. Breskin and N. Zwang, Nucl. Inst. and Meth. 144 (1977) 609.
4. Y. Eyal and H. Stelzer, Nucl. Instr. and Meth. 155 (1978) 157.
5. D.V. Horrach and H.J. Specht, Nucl. Instr. and Meth. 164 (1979) 477.
6. T.C. Awes, C.K. Gelbke, B.B. Back, A.C. Mignerey, K.L. Wolf, P. Dyer, H. Breuer and V.E. Viola Jr., Phys. Lett. Vol. 87B (1979) 43.

Construction of a Position Sensitive Parallel Plate Avalance Counter

T.C. Awes, C.K. Gelbke, G. Poggi and J. Yurkon

Good time resolution at high counting rates with a minimum thickness rendered the Parallel Plate Avalance Counter (PPAC) an almost ideal time-sensitive transmission detector for heavy ions.[1,2] In the last few years techniques have been developed in order to obtain from a PPAC also positon information;[3,4] one of these techniques consist of inserting in the gap between anode and cathode a sense wire plane biased at half the main electrodes potential difference. Delay line read out is used for extracting position information from the signal sensed by these wires that are close to the position of the avalanche. Following the outlined scheme we are building a X and Y Position Sensitive PPAC consisting of two independent elements, one for each direction. The principal characteristic are the following:

sensitive area:	16cm x 20cm
gap between electrodes:	3 mm
distance between adjacent wires:	2 mm
position readout:	tapped delay lines
delay per tap:	2 ns
pressure range:	4-10 torr
filling gas:	isobutane, propane
operating voltage:	500-600 V
expected position resolution:	1 mm

A prototype has been successfully checked at 5 torr propane, 500 V biasing for detecting 5.5 MeV α-particles. Two of these counters will be used for coincident fission fragments detection in connection with the study of light particles emission in central and peripheral heavy ion collisions in the projectile energy range of few tens of MeV/nucleon.[5]

---

1. G. Gaukler, H. Schmidt-Bocking, R. schuch, R. Schube, H.J. Specht and I. Tserraye, Nucl. Inst. and Meth. 141 (1977) 115.
2. A. Breskin and N. Zwang, Nucl. Instr. and Meth. 144 (1977) 609.
3. Y. Eyal and H. Stelzer, Nucl. Instr. and Meth. 155 (1978) 157.
4. D.V. Harrach and J.H. Specht, Nucl. Instr. and Meth. 164 (1979) 477.
5. T.C. Awes, C.K. Gelbke, B.B. Back, A.C. Mignerey, K.L. Wolf, P. Dyer, H. Breuer and V.E. Viola Jr., Phys. Lett. 87B (1979) 43.

On Improving Ge Detector Energy Resolution and Peak-to-Compton Ratios by Pulse-Shape Discrimination

N. Matsushita, Wm. C. McHarris, R.B. Firestone, J. Kasagi, and W.H. Kelly

By studying and discriminating among the (nsec range) rise-times of pulses from Ge γ-ray detectors, we have been able to improve the spectra on two separate levels: First, by discriminating against the slower-rising pulses, the energy resolution and peak-to-Compton ratios can be improved significantly. Figure 1 is an example of this: Gate 1 illustrates a ^{60}Co + ^{152}Eu spectrum resulting from fast-rising pulses; Gate 6, from slow-rising pulses. The improvement is particularly significant (up to 50%) for detectors that have suffered extensive neutron damage. Second, by adding a pulse-height correction to compensate for the effects of varying rise-time, an improved composite spectrum can be obtained without significant loss in detector efficiency. (Figure 1D illustrates this.)

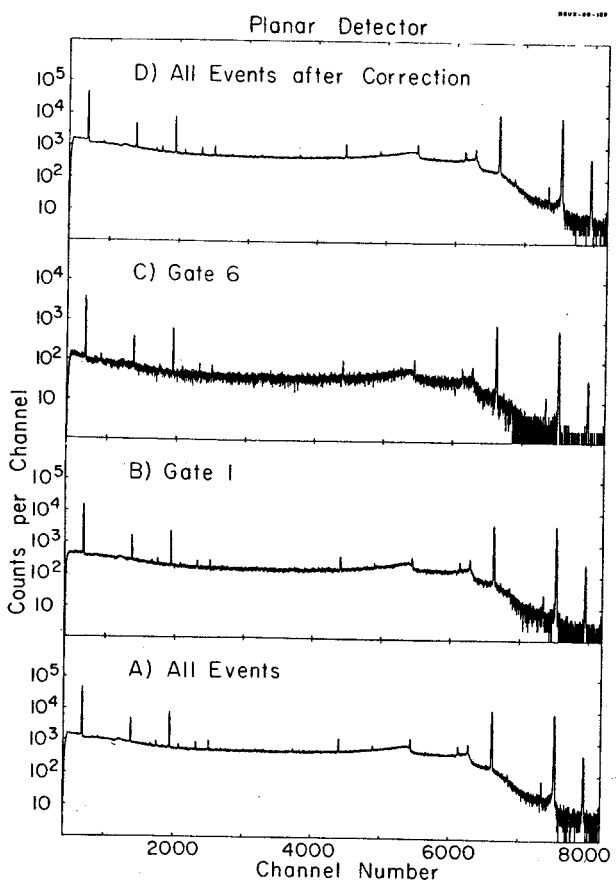

FIG. 1. Rise-time discriminated spectra for ^{60}Co + ^{152}Eu taken with the 2.5% Ge planar detector (see text). The bottom portion A) shows the "all-event" or integral-gated TAC spectrum; B) shows very fast (Gate 1) and C), moderately fast (Gate 6) rise-time spectra; while D) shows the "all-events" spectrum that results from correcting the centroids of the various time-gated slices (see text).

For planar Ge detectors the centroid-shift correction is straightforward: In Fig. 2 we have plotted the centroid of four of the major peaks versus the TAC channel: The peaks are shifted linearly as a function of the rise-time, and the slopes for the lines are energy dependent, being greater for the higher-energy peaks. The slope of the line for each peak can be fitted to

$$A = \alpha E.$$

Here α is a constant and E is the energy. This indicates that the amount of charge trapped in the damaged portions of a detector is proportional to the energy.

This linear dependence makes it easy to develop computer software to shift each pulse-height value by an amount determined by the rise-time and the pulse height. The amount of each shift is given by

$$E_{shift} = AT,$$

where T is the rise-time of the pulse.

After this correction, the "all-events" resolution for the 1332.5-keV ^{60}Co peak improved from 1.84 keV to 1.77 keV FWHM. This is not

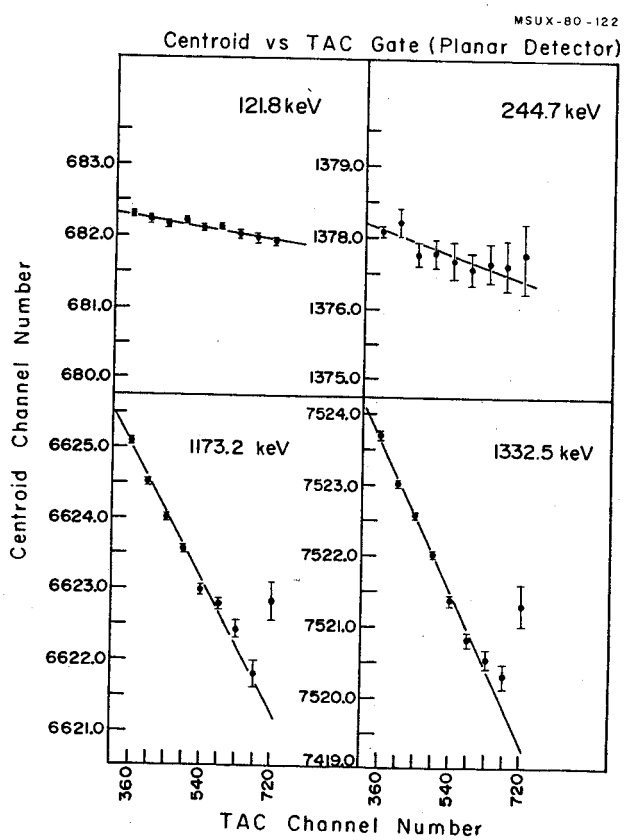

FIG. 2. Plots of the centroids of four of the prominent ^{60}Co and ^{152}Eu peaks as a function of the pulse rise-time.

a remarkable improvement; however, this detector originally had quite good resolution. Had it suffered more extreme neutron damage, we assume that the improvement would have been greater. (Also, in principle, the use of more and narrower rise-time slices should make a further improvement up to limit of time-resolution; here 2-4 nsec is the time limit.)

For coaxial detectors, slow-rising pulses can result not only from neutron-damage "traps" in the detector, but also from the more complicated geometries of the detectors themselves. By measuring two different rise-time components of the pulse we have been able to separate the two effects. For example, a "good-quality" pulse originating from a outer region of the detector and a neutron-damaged "poor quality" pulse originating from a more central region could easily have the same 0.1-0.5 - fraction rise-time, but it is highly unlikely that they would also have the same 0.1-0.7 - fraction rise-time. We have found that the energy pulses can be corrected event by event, using this double rise-time information. Our preliminary results show that we are still able to effect improvements of the order of 50% for those more complicated geometries, without significant loss of efficiency.

RPMS Design and Construction

L. Harwood, J.A. Nolen, Jr., E. Ormand and M. Curtin

One of the major design projects for the Phase II laboratory is the Reaction Product Mass Seperator (RPMS). The primary goal for this device is to separate by mass (m/q) the products of heavy ion reactions induced by the high energy beams from the coupled cyclotrons (up to 200 MeV/A). Measurements of lifetimes and decay properties of nuclei far from β-stability will be done in the focal plane of the seperator. Preliminary ideas on this device were presented in last year's annual report. Since that time the design for Phase II has evolved considerably, but a final design does not yet exist. However, the design of a prototype RPMS for evaluation and use in Phase I has been finalized. The prototype is currently under construction and will be operational sometime in 1981. Progress reports on the construction of the prototype and the design for Phase II are given below. Our design efforts have benefitted greatly from discussions with K.L. Brown (SLAC) and H. Enge (MIT).

Prototype construction

A prototype RPMS has been designed (using the same 5m Wien filter to be used later in the Phase II device) with several constraints which will not exist in Phase II. First, the floor space available within the present building is limited to about 15 m. The only dipole available for the system was one used in the 50 MeV cyclotron beam transport system. Four 8-inch aperture quadrupole singlets were obtained as surplus from SREL (via Brookhaven National Laboratory). Finally, no elaborate second order corrections could be built into this system because at most only one large aperture sextupole is avilable. These constraints led to a design with the component layout shown in Fig. 1. The optics for the system are quite simple. There is point-to-point focusing from the target to the "focal plane" in both the x (dispersive) and y planes. The y envelope is tapered so that it can fit through the small

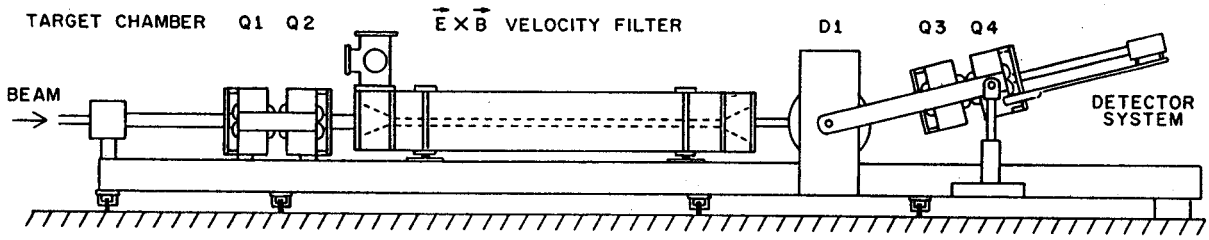

FIG. 1. Side view of component lay-out for the prototype RPMS complete with undercarriage. Pivot point is at right beneath the carriage below the detector box.

Table I

RPMS Parameters (prototype)		
Layout:	QQWDQQ	(W = Wien filter)
Length:	14.3 m	
Max. Energy:	30 MeV/u	
Angular Range:	0^{o} - 30^{o}	
Resolution:	$\frac{M}{M}$ = 100*	(base-to-base) @ 1 msr and 16% energy range
	= 200**	@ 1 msr and 8% energy range

* Calculated for E/A = 20 MeV and M = 2Q with TURTLE.

** Calculated for ^{40}Ca + ^{40}Ca fusion products at E_B/A = 5 MeV (A = 80, q = 18).

(6.25 cm) gap of the dipole. Surprisingly, when the calculations were done the system had quite good characteristics (see Table I).

The problem of changing the scattering angle has been dealt with in a rather novel way. With a 14 m long device, rotation through 30° would require large amounts of floor area. We have chosen to let the beam do most of the moving, as illustrated in Fig. 2. The RPMS carriage is pivoted at the detector-box end or under the dipole as shown in Fig. 1. The centerline is positioned such that it is along a line at $+15^{\circ}$ deflection of the beam by a dipole magnet. If the dipole is turned off, the beam passes straight through it. If the RPMS is rotated slightly, the target again intersects the beam, but now the scattering angle is 15° rather than 0° as it was above. If the dipole deflects the beam by -15°, one can see that the scattering angle becomes 30°. As Fig. 2 shows, this system requires very little target motion (0.5 m) and thus very little floor space. There is the added advantage over the usual "beam swinger" that only one dipole is needed instead of two. This system will also work quite well for Phase II.

All parts of the prototype are in house or designed. The system essentially needs only to be put together on its movable carriage as soon as the latter is built.

Preliminary planning for experiments with the initial version of the RPMS can be done using the information contained in Table I. An example of mass separation as calculated with the beam optics program TURTLE is shown in Fig. 3. This shows the predicted performance in the mass 50 region at ion energies per nucleon of 20 MeV, i.e. 1000 MeV reaction products. Even at this relatively high energy the mass resolving power ($M/\Delta M$) is approximately 100, base-to-base. In addition to the peaks indicated in Fig. 3, however, there will generally be additional peaks due to ions in other charge states but with similar m/q values. For example, assume the peak labelled mass 50 in Fig. 3 represents a fully stripped iron isotope, A=50, q=Z=26, m/q=1.923; a fully stripped manganeze isotope with mass 48 would have an indistinquishable m/q value of 1.920. Such ambiquities must be resolved by the detector system.

A schematic view of a possible detector system for lifetime measurements is given in Fig. 4. In this case the RPMS is tuned for $^{17}C^{6+}$, so that m/q ambiguities also cause $^{17}N^{6+}$ and $^{14}C^{5+}$ ions with the same velocities to enter the detector. At the same velocity the ^{17}N and ^{14}C ions have appreciably less range than the ^{17}C so that the detector thicknesses and/or gas pressures can be adjusted to stop the ^{17}C ions near the plastic scintillators (E_7 and E_8) without interference from the other ions.

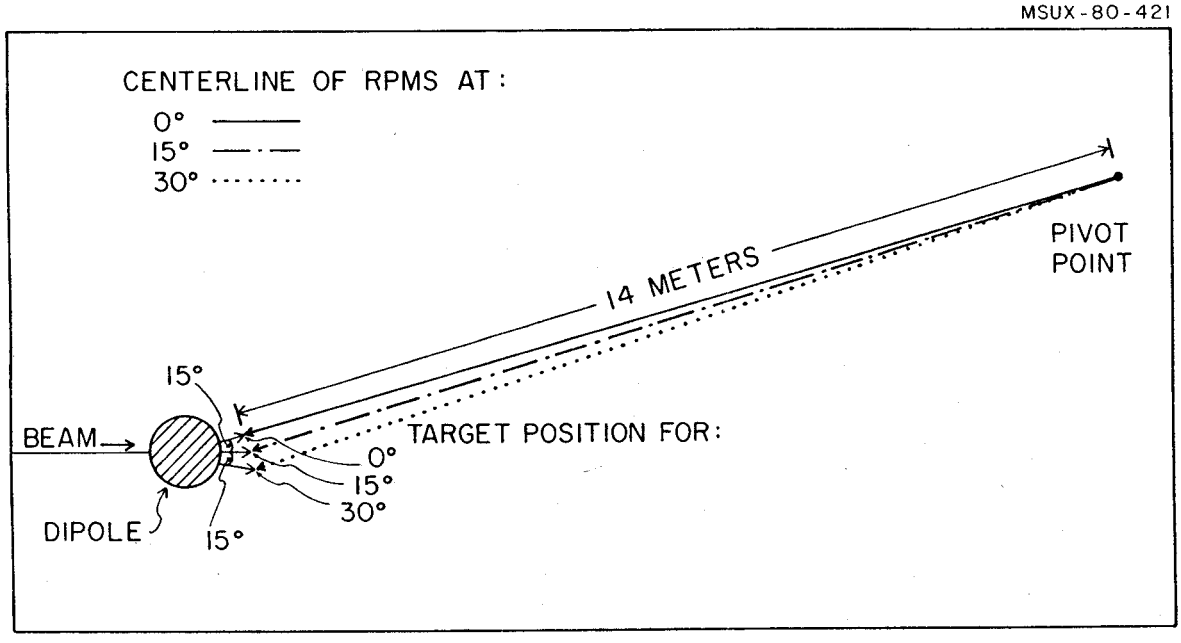

FIG. 2. Illustration of angle-changing technique for the RPMS. RPMS positions for scattering angles of 0°, 15° and 30° are shown.

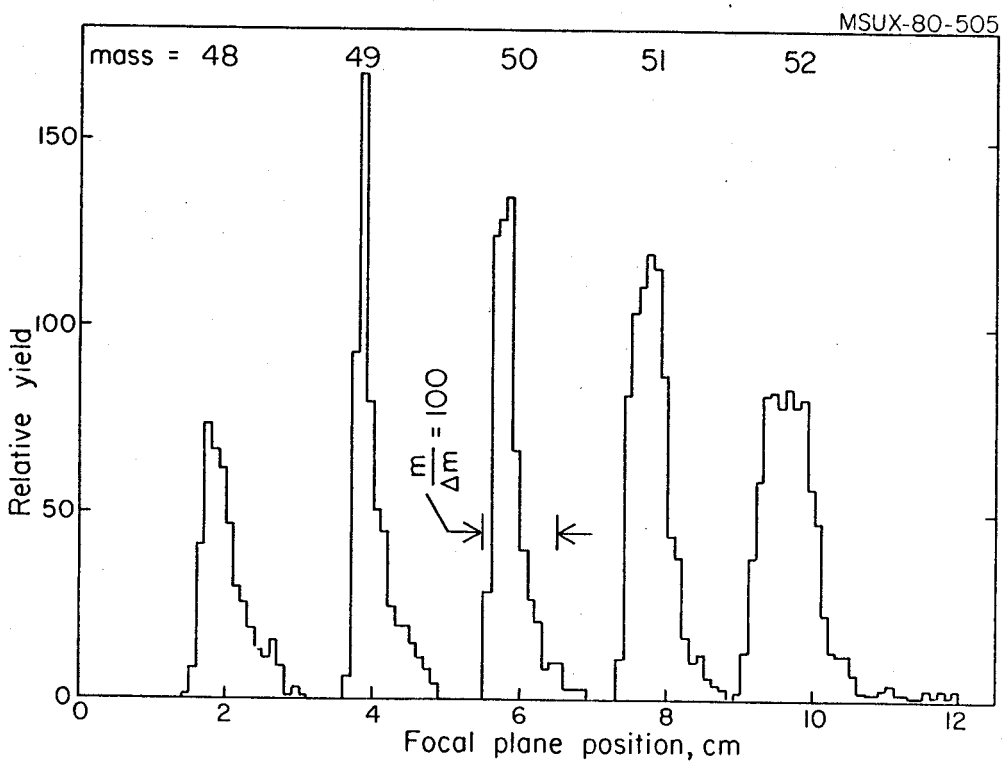

FIG. 3. Monte Carlo spectrum for RPMS. These products have 20 MeV/u. The masses of the particles in each peak are indicated above the peak.

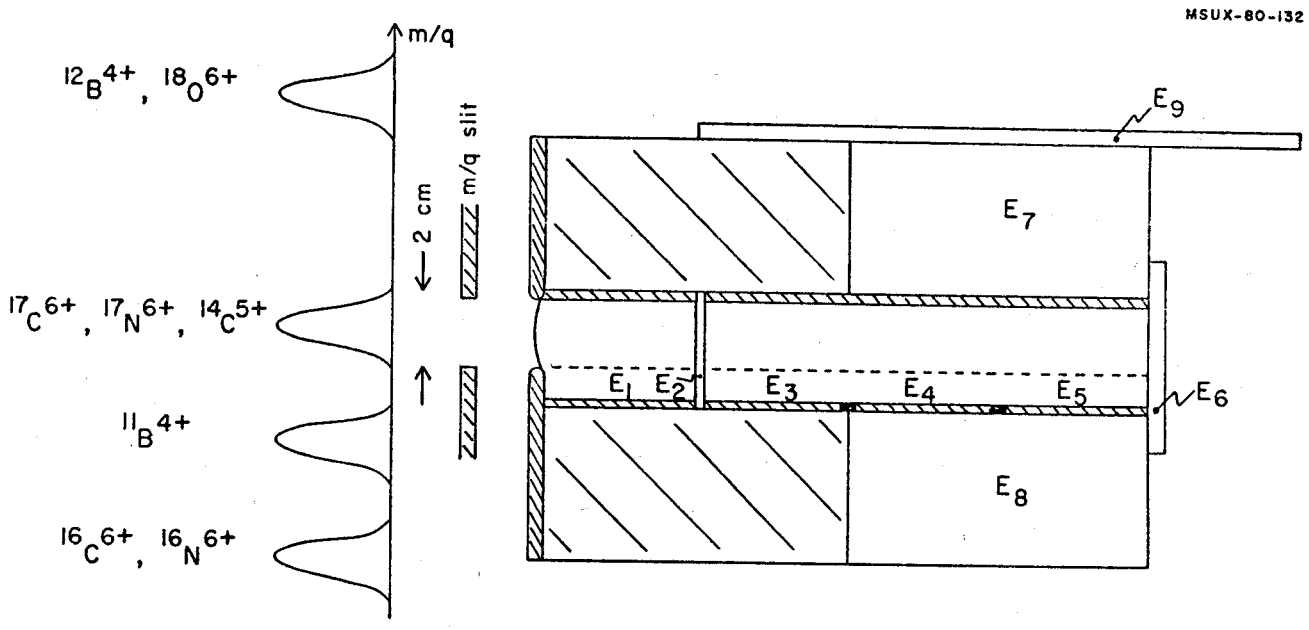

FIG. 4. Possible detector for use with the RPMS for β-decay lifetime measurements. Each independent energy measuring volume is labelled as "E_n".

The experiment to measure the lifetime of ^{17}C can also be used to illustrate count rate estimates for the RPMS. Continum spectra of ^{17}C ions have been observed in bombardments of ^{48}Ca targets with a 100 MeV beam of ^{18}O at the Heidelberg MP tandem. The cross section was measured to be approximately 0.1 mb/MeV-sr at a laboratory scattering angle of 10^{o}. Using this cross section as a known, but possibly passimistic, starting point, yield estimates at the focal plane of the RPMS can be made. Realistic assumptions of target thickness, beam intensity, etc. indicate a lower limit of ^{17}C ions at the detector of 1 to 10 counts/sec. Fragmentation of a ^{22}Ne beam at 40 MeV/u could produce much higher rates.

Phase II

The RPMS design described in last year's annual report has been modified consideralby. Its primary drawbacks were the high quadrupole field strengths needed at high energies (30 kG

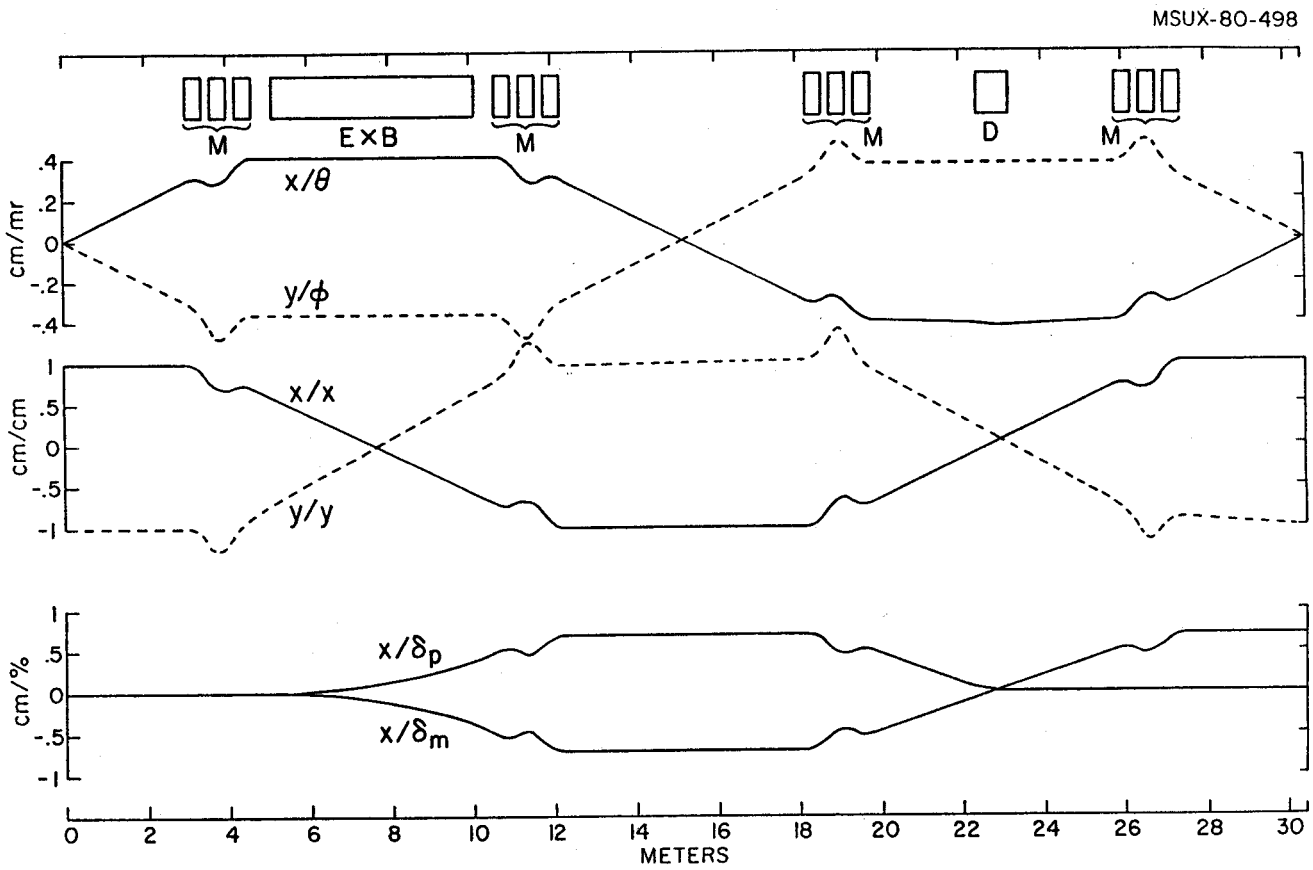

FIG. 5. First-order ray diagram for Phase II RPMS.

Table II

RPMS Parameters (Phase II)

Layout:	M3WM6DM3 (M3 = MMM; $M^{(1)}$ = multipole)
Length:	30 m
Max. Energy:	200 MeV/u (p/q = 1.3 GeV/c)
Solid Angle:	.8 msr[2]
Energy Acceptance:	8%
Dispersion:	8.5 mm/%[3]
Resolution:	$\frac{M}{M}$ = 180 (base-base) @ .8 msr and E = 8% = 320 (base-base) @ .8 msr and E = 2% (3) = 320 (base-base) @ .4 msr and E = 4%

[1]Multipoles are superconducting. Quadrupole field gradient at 1.3 GeV/c is 6.8 kG/in.

[2]0.8 msr requires 8 in. aperture multipoles.

[3]Calculated for E/A = 20 MeV/u and M = 2Q with TURTLE.

at 3" radius for 200 MeV/u) and the lack of a good 3rd order solution. There are presently two new designs under consideration. The first order ray diagram for one of them is shown in Fig. 5; this is the "achromat" layout.

The "achromat" layout is a modification of a series of designs developed for high energy beam transport at SLAC. This new design has a much larger dispersion (8.5 mm/%) than the design reported last year (4.7 mm/%). Also, last year's report gives a line width of 2 mm at 1 msr and 5% velocity bite. This number included first and second order contributions but neglected the large third and fourth order aberrations induced by the very strong sextupoles in that design. Using multipole coupling coefficients as a guide to sextupole placement, it is possible to obtain a perfectly corrected second-order solution for the "achromat". Even though there are no second-order aberrations, there can be significant higher order aberrations created by the sextupoles. The parameters for the current "best" solution are given in Table 2. The second design has a shortened second half relative to the "achromat" layout. Instead of being 30 m long, the second design is 24 m long. The disadvantage of this system is that second-order aberration correction is not as straightforward as with the "achromat" symmetry. Studies of resolution as a function of phase space acceptance are continuing for the various solutions.

Design and Construction of a k=320 Spectrograph for Phase I

J. Nolen, E. Kashy, R. Blue, L. Harwood, A. Zeller and M. Distasio

A simple QQDS spectrograph which can be constructed mostly from existing standard components has been designed and is being assembled for use in the Phase I research program. The existing Enge split-pole spectrograph has a k-parameter of 120, where k is defined by the equation $E/A=k(q/A)^2$. Hence, this spectrograph is not useful for ions with N=Z=q at E/A≥30 MeV. The new spectrograph is designed to remedy this problem by being useful up to 80 MeV per nucleon, i.e. k=320. It is felt that this spectrograph, called the S320, will be very useful for studies of giant resonances in nuclei using the high energy "light" heavy ions from the Phase I cyclotron. It will also be useful for nuclear interaction studies via elastic and inelastic scattering, as well as transfer reactions.

A schematic view of the component layout and the beam envelopes is given in Fig. 1. A plan view of the system as it is to be installed in the experimental area is shown in Fig. 2. The magnetic dipole to be used is a standard High Voltage Corp. MP tandem switching magnet which was obtained from the University of Pennsylvania Tandem Laboratory. The only modification required on this magnet is to change the entrance edge curvature from a radius of -0.3 m (concave) to +0.78 m (convex). When located at zero degrees this dipole also serves as a switching magnet as indicated in Fig. 2.

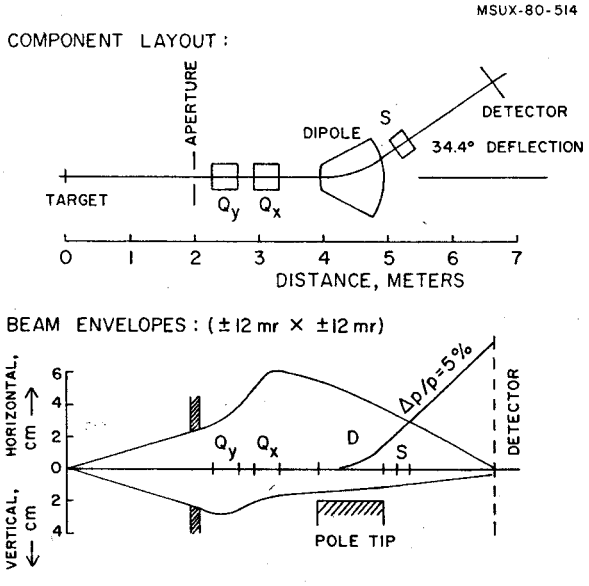

FIG. 1. Schematic view of the component layout of the k=320 QQDS spectrograph (upper) and indication of the amplitudes of the vertical and horizontal particle envelopes through the spectrograph (lower).

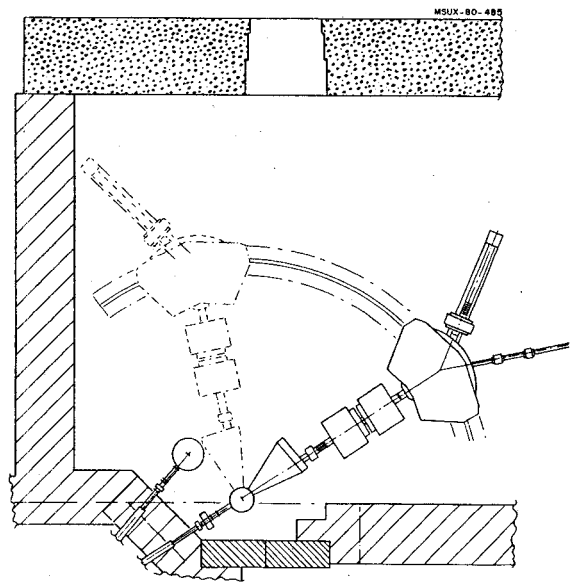

FIG. 2. Plan view of the new k=320 spectrograph in the North Vault of the Phase I experimental area. It is shown in the zero degree position (solid) where it can be used either as a switching magnet or a spectrograph and also in the position (dashed) corresponding to a scattering angle of 70°.

The quadrupole doublet, which has an 8" aperture, became available as a result of the closing of the SREL cyclotron. A precision scattering chamber with a sliding seal has been obtained on loan from the University of Minnesota. This chamber was originally constructed for elastic scattering studies by Professor G. Greenlees at Minnesota. This chamber will also be useful as a stand alone device, i.e. independent of the spectrograph, as well as for coincidence studies using the spectrograph. The sextupole magnet for this spectrograph has been designed and is currently under construction. It is a scaled-up version (6" aperture) of the 3" and 4" sextupoles used in the beam transport system of the k-50 cyclotron, but it will use hollow, water-cooled conductor rather than the solid, air-cooled wire used in the smaller sextupoles. The pole tip of the new sextupole will also have an improved shape determined via a conformal mapping calculation. The carriage and rail system for this spectrograph have been designed and the components are currently being procured. The detector system has been designed and the first module constructed and tested as described in the detector lab section of this annual report. The

Table I. Parameters of the QQDS k=320 spectrograph.

Dispersion:	D_x = 1.6 cm/% ($\Delta p/p$)
Magnification:	M_x = -0.67 (D/M = 2.4)
	M_y = -2.5
Beam spot on target (assumed):	
	0.5 mm incoherent width
	3 mm tall, dispersion matched
	2.4 mm dispersed beam width for 0.1% beam energy spread
Solid angle:	
	$\Delta\theta$ = 8 mr
	$\Delta\phi$ = 12 mr
	Ω = 0.3 msr
Calculated line width (ray tracing):	
	$\Delta E/E \leq 0.1\%$, 0.8 mm
Range:	$\Delta E/E$ = 20%
	60 MeV at 300 MeV
Focal plane:	Normal incidence, 16 cm long x 2.6 cm tall
Max rigidity:	$B\rho_{max}$ = 2.57 T-m @ 1.47 T
	ρ_{max} = 1.75 m

important optical and magnetic parameters of this QQDS spectrograph are given in Table I. This spectrograph will be operated in the energy-loss, or dispersion-matched mode. Kinematics effects due to the angular divergence of the beam will be compensated for by "beam-matching" of the transport system. The kinematics effects due to the finite angular acceptance of the spectrograph can be compensated for by refocussing of the quadrupole doublet according to the kinematic parameter of the reaction. Alternatively, if the detector system is set up to measure the scattering angle, then computer correction for kinematic shifts can also be done.

Beamline Vacuum Systems Development

R. Blue, K. Beard and E. Kashy

For Phase I operation with the K500 cyclotron the transport of heavy ions has required the upgrading of beamline components to provide improved vacuum conditions. However, cost considerations require that extensive use be made of existing beamline components. Beamlines for the K50 cyclotron had employed aluminum piping with V-band couplings at O-ring sealed joints. Slit jaws, viewers, beam stops, etc. were mounted as modular units on beam boxes of a standard laboratory design. This basic system has been preserved in the K500 beamline design so that many components can be reused.

A significant improvement in operating vacuum has required a reduction in the amount of organic materials exposed to the vacuum. Of particular importance in this regard is the elimination of all the sliding shaft seals that were previously employed in beam box modules and gate valves. New gate valves have been purchased and new beam box modules designed and constructed which have stainless steel bellows to seal sliding shafts. Further reduction in vacuum system gas loads is to be achieved by the replacement of O-rings by metal seals. Two types of seals have been tested extensively as direct replacements to fit O-ring grooves. These include commercially available metal C-rings and seals designed in house which employ indium wire. Extensive tests of indium seal designs have been conducted to insure reliability of the designs finally selected.

On new components where indium seals need not involve an O-ring groove, indium wire 0.030 or 0.040 inches in diameter is retained by pressing it into a groove nominally 0.020 by 0.020 inches which is cut in the face of one of the mating flanges. Since the indium wire is then retained in the correct position even if the flange is inverted, reliable sealing is achieved. On large flanges a torque wrench is used to insure uniform and continuous loading on the bolts that compress the indium seal.

In the case of the V-band coupling between beamline pipe sections, the sexless flanges had previously been sealed by an O-ring on an aluminum retaining ring which together filled a space symmetrically divided between the two mating flanges. In this situation, the metal seal design consists of an aluminum ring with indium seals on both faces of the ring which then serves as a direct replacement for the O-ring and retainer. As described above, the indium wire is retained in a small groove cut in the aluminum ring. In the vicinity of a beam box, where the total surface area of O-rings exposed was relatively large, conversion to metal seals results directly in a factor of 10 or more improvement in the vacuum.

An additional consideration in the selection of beamline materials relates to the residual radiation induced by the higher energy beams to be available from the new facility. In beam tests conducted by Richard Pardo and Peter Miller aluminum is clearly to be favored over the commonly considered alternative, stainless steel. Specifically the best choices appear to be either pure aluminum (1000 series) or copper-free alloys (6000 series). It is not felt that the better vacuum properties of stainless steel offset the advantages of aluminum in this regard.

The major beamline components yet to be described are the wall plugs and the magnet chambers. The wall plugs serve to block beam pipes to prevent the transmission of radiation through unused beam ports in the shielding wall. The existing beam plugs have been vacuum hardened by replacing the O-ring flange seal on the box by an indium wire seal and by adding a bellows to seal the actuator shaft. The magnet chambers for the large dipole magnets are among the largest beamline components requiring all new design and construction. The designs, which incorporate large pumping ports to insure good vacuum conditions, are being constructed in house by welding aluminum plate.

The selection of vacuum pumps for the beamlines and for experimental chambers was determined by the need to greatly reduce residual hydrocarbons in the vacuum. Triode ion pumps will be placed at intervals along the beamline where pumping speeds become conductance limited. Where gas loads are larger, closed-cycle cryopumps and ion pumps in combination may overcome some of the disadvantages associated with either type operating alone.

Two additional types of pumps will be used primarily for roughing operations. A number of mobile pumping carts, each equipped with a small turbomolecular pump and a mechanical backing pump will be available for roughing beamlines and chambers as required. These systems are designed to minimize possible backstreaming from the oilsealed backing pump during the roughing operation. These systems, however, do not provide adequate pumping speed in the range above 1 Torr for pump down of large volumes such as the 60-inch scattering chamber. Specifically for the initially pumping phase of large volumes, high speed Roots blower systems will be used.

While it would obviously be desirable to convert to metal seals throughout all experimental vacuum systems, there are clearly situations where the benefits cannot justify the difficulty of the conversion. In these locations Buna O-rings are being replaced by Viton as an improvement that can be easily accomplished.

Other materials employed in vacuum chambers, insulators for example, are being screened to eliminate those which have excessive outgassing rates. For this purpose, a program of vacuum testing of components and materials is being continued throughout the construction phase of the beamline.

Beam Transport Calculations for K500 Cyclotron Operation

J. Kasagi, S. Angius and E. Kashy

In this report, we present the result of the calculation for the beam transport of the experimental facility using the K500 cyclotron.

The layout of the experimental floor with beam transport elements is shown in Fig. 1. As can be seen, the experimental area is separated into two large room designated North and South. The North vault houses the Enge split pole spectrograph, an S320 spectrograph capable of bending the most rigid beams, a scattering chamber for neutron experiment, a low rigidity beam line and the counting apparatus for the cryogenic helium-jet apparatus.

is the provision for a variable linear and angular dispersion at the magnetic spectrograph target in order to accomodate matching conditions in the "energy-loss" mode for the wide variety of reactions and detection systems which will be utilized.

The design of the beam transport system is strongly influenced by an unusual feature of the extraction system of the K500 cyclotron, namely that the extraction system consists entirely of inert focusing elements. This feature greatly simplifies design and construction of the extraction system itself but at the cost

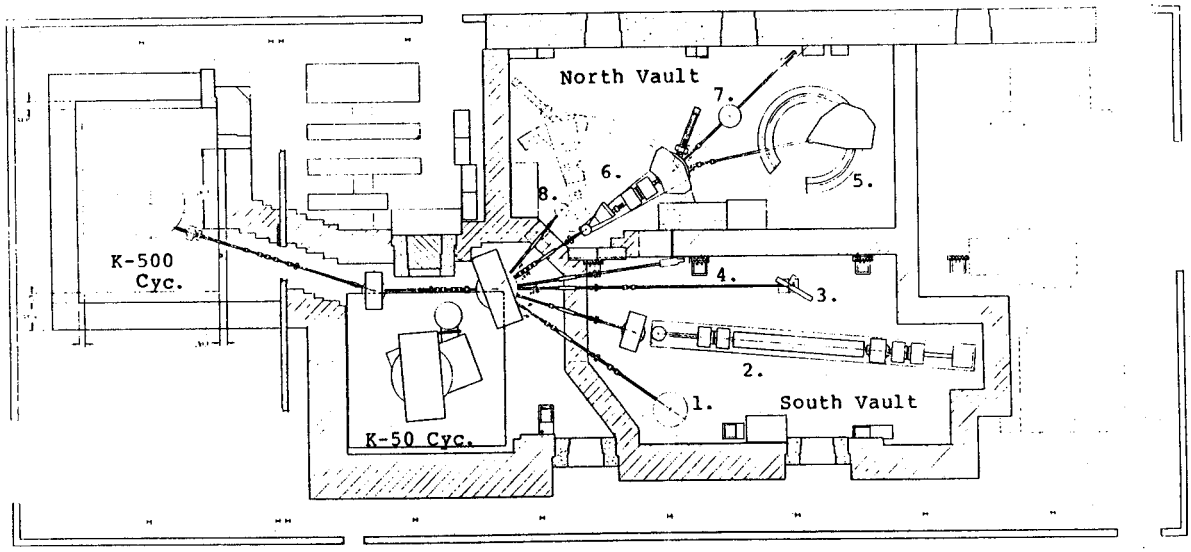

FIG. 1. Layout of the experimental floor. 1. 60 inch Scattering Chamber. 2. Recoil Product Mass Separator. 3. γ-ray Goniometer. 4. Cryogenic He Jet. 5. Enge Split-pole Spectrograph. 6. S320 Sepctrograph. 7. Neutron Scattering Chamber. 8. K=250 beam line.

The South valult houses the 60 inch scattering chamber, an initial version of the recoil particle mass separator (RPMS), a gamma ray goniometer and the target for the cryogenic helium-jet apparatus.

The beam transport calculation has been carried out for all the beam courses and the arrangement of beam transport element was designed to accomodate the wide variety of beams expected from the K500 cyclotron. Calculations to design this system include ray tracing in the fringing field region of the cyclotron (where special measurements were made) and conventional matrix methods for the rest of the beam line. A major design feature of the system

of a variability in direction and focusing conditions for beams leaving the cyclotron. (The basic cause of this phenomenon is the fact that the inert extraction system focusing elements stay at fixed absolute strength whereas bending and focusing effects of the fringe field vary in proportion to main field strength.) The first section of the transport system must then be used as an active element to compensate for this variability in order to bring all beams to an approximately identical phase space condition at the location of the first slit. Figure 2 shows an example of two extreme beams tracked through this portion of the optical system, the quantity plotted being the horizontal and

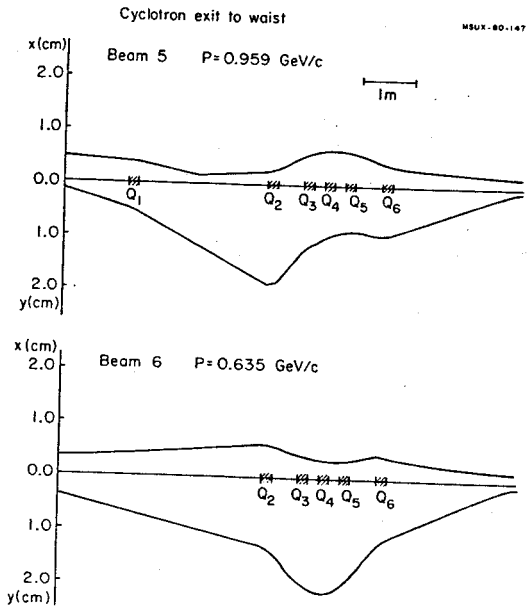

FIG. 2. Plot of horizontal and vertical beam envelopes from the cyclotron exit to the waist located at the first defining slit. The two beams represent the extreme limits of the distribution of focusing conditions for beams leaving the cyclotron. With appropriate adjustments of the six quadrupoles, the beams are brought to an approximately identical focusing condition at the first slit which would be located at the right edge of the figure.

vertical envelope of the beam as a function of path length through the system. "Beam 5" has a momentum of 0.959 GeV/c, "beam 6" has a momentum of 0.635 GeV/c and both have Q/A = 0.322. Transport parameters of these beams at the cyclotron exit location are much different as listed in Table 1. Obtained beam parameters at the initial waist location are also listed in Table 1 for these two beams. As can be seen, the beam transport system in this region includes sufficient optical elements to allow compensation for the variable emittance condition from the cyclotron, while at the same time keeping the beam envelope within reasonable limits ($\leq$ 2 cm).

The beam parameters for "beam 6" at the target locations of various beam lines are summarized in Table 2. The values of R_{16} for the Enge split pole and the S320 target locations satisfy the linear dispersion matching condition for each spectrograph. Almost same beam parameters at the target locations can be realized for "beam 5".

Table 1. Beam parameters in first section of transport line. "x" and "θ" are the maximum values of horizontal displacement and divergence for particles, "y" and "ϕ" are the similar quantities for the vertical displacement and "R_{16}" and "R_{26}" give the displacement in direction and angle per % momentum variation relative to the central ray.

	x(cm)	θ(mr)	y(cm)	ϕ(mr)	R_{16}(cm/%)	R_{26}(mr/%)
Beam 5						
at cycl exit	0.49	0.85	0.12	3.25	-18.12	15.04
initial waist	0.20	1.41	0.08	3.77	7.32	-22.21
Beam 6						
at cycl exit	0.34	0.89	0.36	2.5	-0.96	21.37
initial waist	0.16	1.54	0.10	4.61	4.78	-16.26

Table 2. Beam parameters at the target locations for various beam lines (Beam 6).

	x(cm)	θ(mr)	y(cm)	ϕ(mr)	R_{16}(cm/%)	R_{26}(mr/%)
Low rigidity	0.43	3.38	0.45	4.77		
S320	0.04	6.72	0.13	3.54	-2.19	67.54
Split pole	0.05	4.53	0.24	2.10	4.61	-44.91
Neutron Chamber	0.06	3.93	0.12	3.69		
He jet	0.22	1.20	0.42	1.18		
γ-ray	0.09	2.85	0.22	2.11		
RPMS	0.34	1.00	0.07	6.75		
Scatt. Chamber	0.12	1.99	0.22	2.08		

Status of the K=800 Spectrograph Design

A. Zeller, J. Nolen, L. Harwood and E. Kashy

The design of a k=800 spectrograph (S800) to be used with the Phase II Cyclotrons has evolved considerably since the preliminary description given in last year's annual report. The most significant development is an increase in the solid angle from 5 to 20 msr. The present optical design and a preliminary report on the dipole field calculations are given below.

Because the accelerator has a non-zero energy spread (0.1%) which is much larger than the desired experimental energy resolution (0.01%), it is necessary to operate the system in the dispersion-matching or energy loss mode. In this mode the resolving power (D/M) of the beam dispersive or "beam analyzing" section is as important or more important than that of the spectrograph. An energy-loss system and overview of the S800 pit are shown in Fig. 1. In this example the dispersions are in the vertical plane and the beam dispersive section includes the two 45° bends on the left side of the figure.

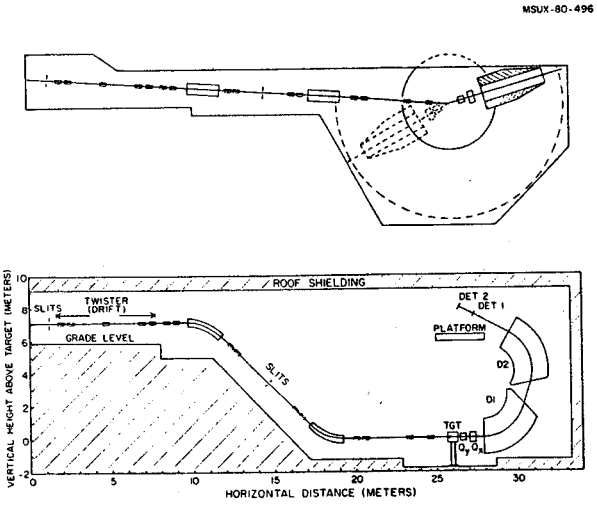

FIG. 1. Top and side of the beam analysis system and S800 spectrograph.

A phase space matching system consisting of a quadrupole quartet images the beam on the target and a QQDD spectrograph follows the target. The present example also includes a phase space rotator located in the first drift section of the beam dispersion system, labeled TWISTER in Fig. 1. This quadrupole qunitet interchanges the horizontal and vertical phase spaces when turned on, and is optically equivalent to a drift otherwise. (The quadrupoles are rotated 45° from the normal orientation.) Hence, the phase space rotation is optional and the choice is dictated by the particular experimental requirements. Typical phase space ellipse areas for the MSU superconducting cyclotrons are likely to be 1 mm-mr horizontally and 5 mm-mr vertically. With spectrograph dispersion in the vertical plane, better energy resolution is possible if the 1 mm-mr phase space is rotated into this plane. On the other hand, if angular resolution (measured horizontally) is the dominant experimental consideration, then it is best not to energize the TWISTER.

The spectrograph mode chosen was vertical (VHV), mainly in consideration of the ease in tuning and the decoupling of the scattering angle and dispersion measurements. In this mode the scattering angle is derived from the horizontal readout of a two dimensional position sensitive focal plane detector while the momentum measurement comes from the vertical position. Two detectors, one meter apart, provide the angular information necessary for ray tracing. A side view of the spectrograph is shown in Fig. 2. The quadrupoles and edge angles provide the necessary first order focussing while edge curvatures will be used for second and higher order corrections. The edge curvatures provide a reduced requirement for orbit reconstruction calculations and hence permit higher counting rates in the computer.

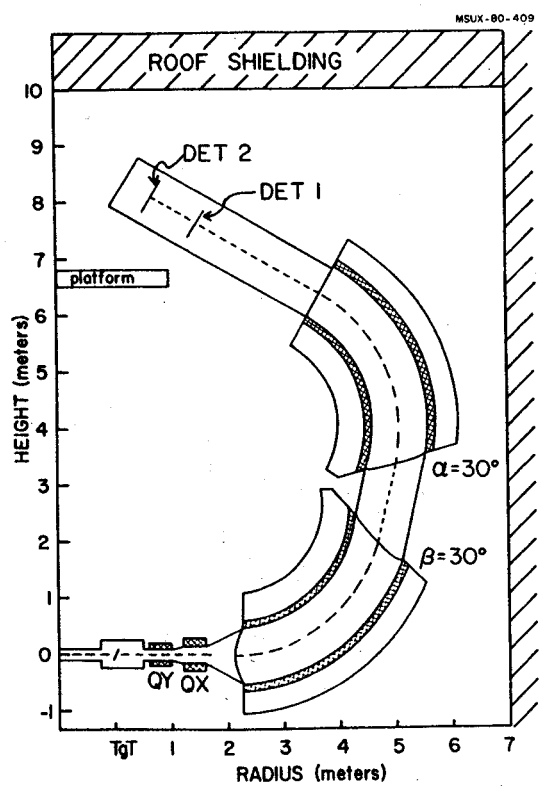

FIG. 2. Side view of the S800 spectrograph.

Table I. Parameters of the K=800 Spectrograph

Energy Resolution:	$\Delta E/E=10^{-4}$ with 1mm radial object size for beam analysis system
Energy Range:	$\Delta E/E=10\%$
Solid Angle:	Ω = 20 msr
Resolving Power:	D/M = 11.7
Radial Dispersion:	D = 9 cm/%
Radial Magnification:	M = 0.78
Axial Dispersion	R_{34} = 0.74 mm/mr
Angular Resolution:	$\Delta\theta \leq$ 2 mr (total of beam plus spectrograph contributions)
Focal Plane Size:	50 cm (Radial) x 15 cm (Axial)
Focal Plane Tilt:	15^{o}
Magnetic Rigidity:	B_{ρ} = 4 T-m
Dipole Fields:	B = 1.5 T (ρ = 2.7 m)
Dipole gap:	D = 15 cm
Dipole Size:	2 of 3.5 m long x 100 cm wide (75^{o} bend)
Weight of Dipoles:	Approx. 100 tons each
Quad Sizes:	#1 20 cm ID x 40 cm long
	#2 25 cm x 15 cm x 40 cm
Detector Requirements:	Two 2-Dimensional det., 1m separation
	#1 50 cm x 15 cm
	#2 62 cm x 16 cm
	Resolution: Radial 0.2 mm
	Axial 0.5 mm

Detailed ray tracing calculations for all orders have been carried out and a beam envelope for one of the solutions is shown in Fig. 3. Because the design of the magnet and the optics calculations are not independent, that is they interact, dipole field calculations using the relaxation code POISSON* have been carried out. A modified window frame design has been chosen since it seems to give the required field characteristics with the least amount of steel. The end view of a promising design is shown in Fig. 4. The field and the gradient of the field for this case are shown in Fig. 5. It was found that a magnet which produced a flat field to 1 in 10^4 over a 70 cm width was prohibitively expensive.

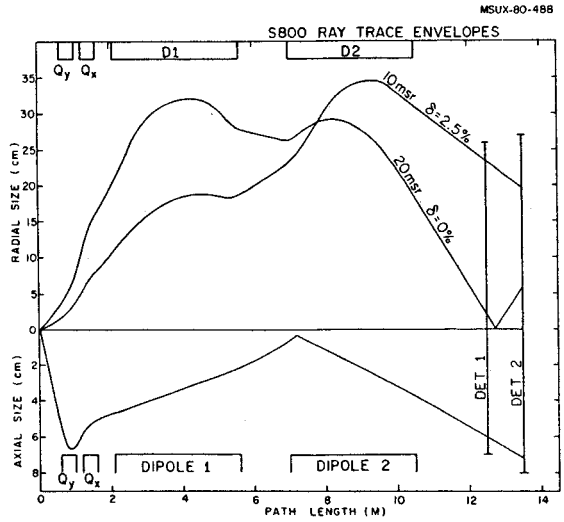

FIG. 3. S800 particle envelopes.

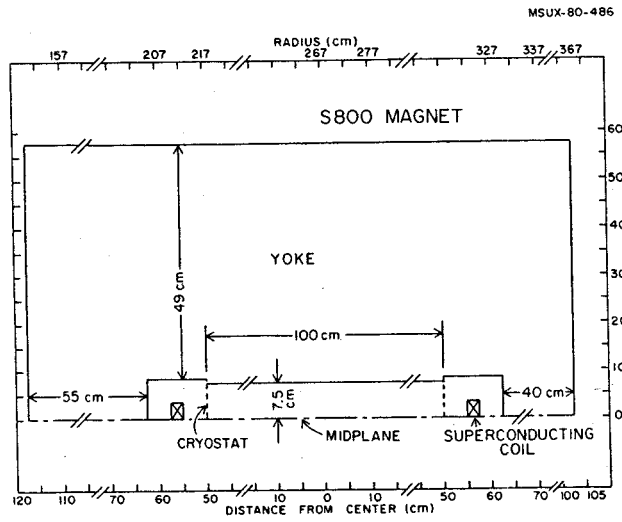

FIG. 4. S800 dipole cross sections.

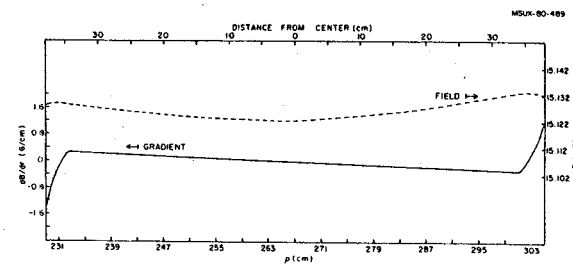

FIG. 5. Plots of the magnetic field and field gradients design shown in figure 4.

However, a smooth gradient, such as that in Fig. 5, would be permitted and corrected by edge curvatures and ray tracing. In fact, a 1 G/cm gradient at 35 cm from the center is a sextupole component which helps reduce some of the second order aberrations.

Table 1 lists the design goals and characteristics of the spectrograph. It should be pointed out that such things as the widths of the return yoke and the edge curvatures are not finalized, and will be fine tuned when coil and cryostat designs have been completed.

*R.F. Holsinger, program POISSON (unpublished) 1979.

The Pre-operational Environmental Surveillance Program at the NSCL

S. Carvalho, G.M. Crawley, E. Kashy and W. Malchman*

Many objectives for environmental surveillance programs have been expressed before.[1,2,3,4] According to Denham,[5] the 4 primary purposes are:

"1) to assess the actual or potential radiation dose to persons in the site environs.

2) to test the compliance or non-compliance of observed data with standards and regulations expressed in annual doses.

3) to verify that effluent controls are adequate and have not deteriorated and

4) to check for long term build up and to predict environmental trends from plant released radioactivity."

In order to fully understand the results of an environmental program during the operational phase of a nuclear facility, baseline environmental data are needed for comparison with later operational studies. Therefore a pre-operational program was established for the NSCL with the purpose of assessing "background" levels and their variations in environmental media, in the area surrounding the laboratory.

The study was conducted based on the two population exposure pathways considered the most important, which are the air and water.

Air Sampling

The atmosphere sampling was performed by using two low volume air samplers. Each sampler was randomly assigned to a locaton every week, so that, at the end of a nine week period, the background radioactivity level could be determined at all the chosen locations. The air samplers were continuously operated for a week before the filter was collected.

The locations selected, numbered from 1 to 6 are shown in Figures 1 and 2. Location 7, chosen as a suitable "control" location, in the prevalent upwind direction, is about 15 miles southwest of the NSCL, at Holt High School.

The equipment used for filter analysis consisted of a low background proportional counter operating at 43% efficiency (β_{max}=0.546 MeV) and 32% alphas efficiency (5.48 MeV max). For gamma ray detection a Ge(Li) detector was used and a mixed radionuclide gamma ray standard was used for the gamma-system absolute calibration.

The filters were counted on the Ge(Li) detector for short and long-lived radionuclides and gamma-ray analysis was performed by using a fitting program (SAMPO).[6] The gamma-ray spectrum collected for each filter analyzed was studied and due to the similarities found among them, one was chosen as representative of the time period and locations being sampled.

The blank filters were previously counted and the radionuclides originally present were measured so that the amounts found would be subtracted from the quantities detected after sampling was performed. Results are presented in Tables 1 and 2. Figure 3 shows the gamma-ray spectrum for the filter sample. Average amounts of ^{60}Co and ^{40}K were too close to that originally present in the blank filter to be considered as part of the radionuclides contributing to the air activity levels.

Gross alpha and beta counting were performed 27 hours and 2 days after the end of the weekly sampling period respectively. Repression analysis results showed no significant difference among either locations or week periods tested. Therefore, statistically one can say that the best estimates of the mean gross beta and alpha concentrations on the filters, are the mean values, which are $2.0 \times 10^{-2} \pm 2.2 \times 10^{-3}$ pCi/m^3 and $6.2 \times 10^{-3} \pm 7.7 \times 10^{-4}$ pCi/m^3 respectively. The control location was not included in the mean value determination.

Water Sampling

The water sampling was performed at two different locations at the Red Cedar River. The purpose of such sampling was the determination of any long-lived contaminants present in the river at the time of sampling or the background levels of the samples if no contamination was found.

Surface water grab samples (3.5 liters each) were collected from two locations (A and B) as shown in Fig. 1. Sampling was performed once a week at both locations for a period of 4 weeks. The water was evaporated on a 2 inches planchet for gamma isotopic analysis and gross beta counting, carried out 5 and 6 days after collection for betas and gammas respectively.

The results of the analysis of variance performed on the gross beta data showed no significant difference among the locations and weeks when sampling took place. Therefore, one can say that the best estimate of the mean gross beta concentration in the surface water collected is the mean value, which is equal to $19 \times 10^{-1} \pm 1.5 \times 10^{-1}$ pCi/l.

The spectrum collected for each planchet was analysed. The fitting program SAMPO[6] was used. Figure 4 shows the Ge(Li) deflector spectrum of gamma-rays. Gamma-ray emitting radionuclides concentration detected at locations

Figure 1. Air and Water Sampling Stations.

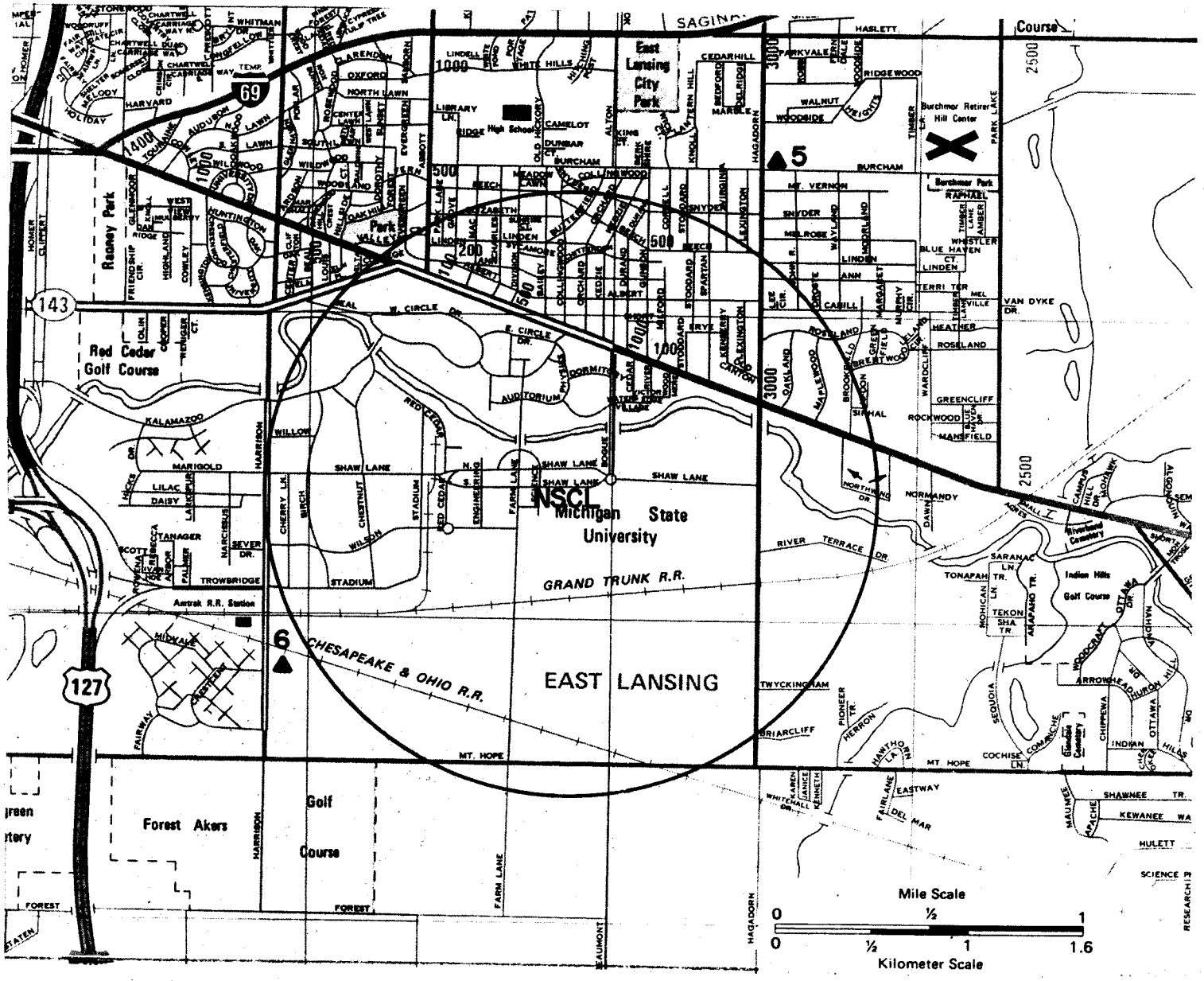

Figure 2. Air Monitoring Stations No. 5 and 6.

Table 1. Radionuclides identified by "location".

LOCATION[b]	AVERAGE CONCENTRATION (pCi/m^3) ± ERROR[a]			
	^{40}K	^{60}Co	^{137}Cs	^{7}Be
1*	1.4(E-1)±1.0(E-2)	5.5(E-2)±8.0(E-3)	ND[c]	1.1(E-2)±2.3(E-3)
2	1.2(E-1)±1.6(E-2	5.1(E-2)±5.5(E-3)	ND	8.4(E-2)±2.2(E-3)
3	1.2(E-1)±1.1(E-2)	5.9(E-2)±5.5(E-3	1.5(E-2)±2.4(E-3)	9.2(E-3)±2.8(E-3)
4*	1.2(E-1)±1.4(E-2)	5.1(E-2)±9.9(E-3)	ND	1.2(E-2)±1.9(E-3)
5+	1.4(E-1)+7.3(E-3)	5.5(E-2)±5.1(E-3)	ND	1.1(E-2)±2.1(E-3)
6	1.3(E-1)±5.1(E-2)	4.4(E-2)+6.2(E-3)	ND	9.5(E-3)±2.9(E-3)
7+	1.3(E-1)±9.8(E-3)	3.7(E-2)±4.4(E-3)	1.8(E-2)±1.5(E-3)	1.5(E-2)±4.4(E-3)

a The error term represents only the error in the peak area, given by the fitting program used.

b Numbers represent averages of 3 filters per location unless specified by *, meaning 2 filters or +, meaning only 1.

c ND = not detectable. It means that the fitting program used was not able to fit a Gaussian to the peak even though it was seen in some of the cases in the spectrum plotted. In those cases usually the statistics were very poor.

Table 2. Radionuclides identified by "week".

WEEK[b]	AVERAGE CONCENTRATION (pCi/m^3) ± ERROR[a]			
	^{40}K	^{60}Co	^{137}Cs	^{7}Be
3	1.2(E-1)±1.5(E-2)	5.5(E-2)±1.2(E-2)	ND[c]	8.8(E-3)±1.9(E-3)
4	1.4(E-1)±1.7(E-2)	5.1(E-2)±1.0(E-2)	ND	1.0(E-2)±3.1(E-3)
5	1.2(E-1)±1.5(E-2)	5.1(E-2)+7.3(E-3)	ND	9.5(E-3)±3.1(E-3)
6	1.2(E-1)+1.1(E-2)	ND	1.5(E-2)±2.4(E-3)	9.5(E-3)±2.0(E-3)
7	1.8(E-1)±5.1(E-2)	ND	ND	1.1(E-2)+2.2(E-3)
8[d]	1.3(E-1)±8.4(E-3)	ND	ND	ND
9[d]	1.2(E-1)±7.0(E-2)	ND	ND	ND
10	1.3(E-1)+9.9(E-3)	3.7(E-2)±4.4(E-3)	1.8(E-2)±1.5(E-3)	1.5(E-2)±4.4(E-3)

a The error term represents only the error in the peak area, given by the fitting program used.

b Numbers represent averages of 2 filters per week.

c ND = not detectable. It means that the fitting program used was not able to fit a Gaussian to the peak even though in some of the cases, it was seen in the spectrum plotted. In those cases usually the statistics were very poor.

d data shown represent only 1 filter.

Table 3. Radionuclides Concentrations Detected by "Location".

	Concentration (pCi/l ± error)[a]	
	LOCATION	
	A	B
^{40}K	2.1(E+1)±3.5	2.2(E+1)±2.9
^{60}Co	4.8±1.6	5.9±1.6
^{137}Cs	3.6+0.6	4.0±0.6

a The error term represents only the error in the peak area, given by the fitting program used.

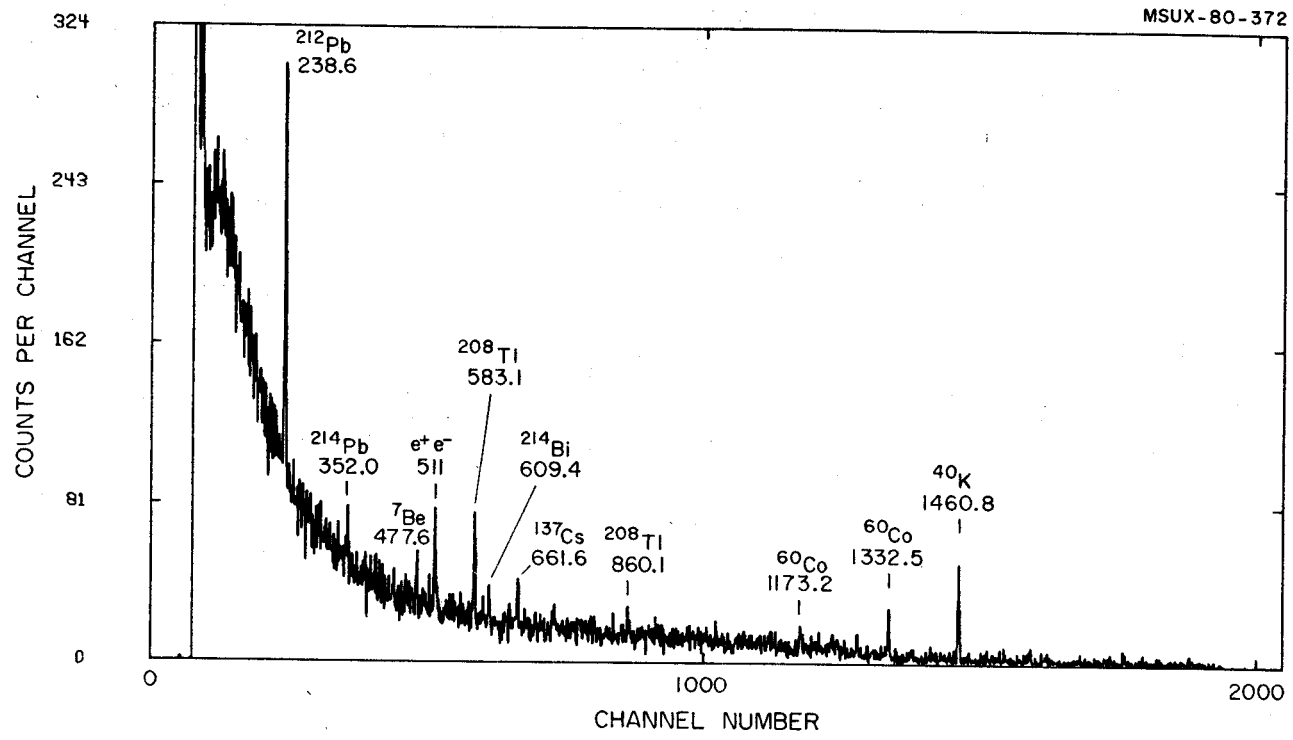

Figure 3. Ge(Li) Detector Spectrum of Gamma-Rays for the Filter Sample

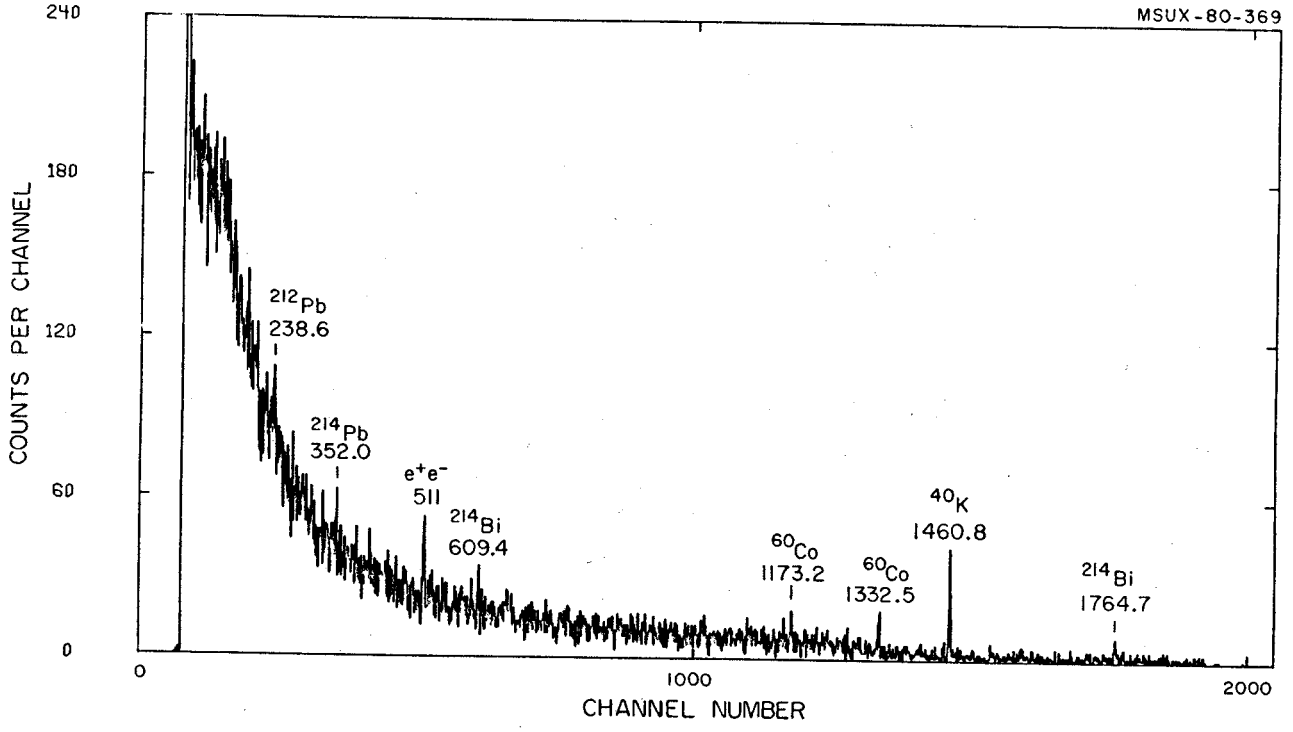

Figure 4. Ge(Li) Detector Spectrum of Gamma-Rays for the Water Sample.

A and B are presented in Table 3. Results of comparisons between the ^{40}K detected in both sample and blank planchet used show that no significant differences are observed.

Due to the many factors controlling the variability of the natural radioactivity detected in the water samples, only identification was performed for such peaks.

A more complete discussion of this Survey is contained in a Report MSUCP-34, August 1980.

* Office of Radiation, Biological and Chemical Safety.

1. U.S. Environmental Protection Agency, 1972, "Environmental Radioactivity Surveillance Guide", ORP/SID 72-2.
2. U.S. Energy Research and Development Administration, 1977, "A Guide for Environmental RAdiological Surveillance at ERDA Installations", ERDA 77-24.
3. National Council on Radiation Protection and Measurements, 1976, "Environmental Radiation Measurements", NCRP Report No. 50.
4. U.S. Nuclear Regulatory Commission 1975, "Programs for Monitoring Radioactivity in the Environs of Nuclear Power Plants", Revision 1, Regulatory Guide 4.1.
5. Denham, Dale, H., 1979, "Environmental Radiological Surveillance in Perspective: The Relative Importance of Environmental Media as a Function of Effluent Pathway and Radionuclides", Health Phys. 36,273.
6. Routti, J.T. and Prussin, S.G., 1969, "Photopeak Method for the Computer Analysis of Gamma Spectra from Semiconductor Detectors",